Modeling and Analysis of MmWave V2X Networks With Vehicular Platoon Systems

Wenqiang Yi, *Student Member, IEEE,* Yuanwei Liu, *Senior Member, IEEE,* Yansha Deng, *Member, IEEE,* Arumugam Nallanathan, *Fellow, IEEE,* and Robert W. Heath Jr., *Fellow, IEEE*

***Abstract*—Due to the low traffic congestion, high fuel efficiency, and comfortable travel experience, vehicular platoon systems (VPSs) become one of the most promising applications in millimeter wave (mmWave) vehicular networks. In this paper, an effective spatial framework for mmWave vehicle-to-everything (V2X) networks with VPSs is proposed by utilizing stochastic geometry approaches. Base stations (BSs) are modeled by a Poisson point process and vehicles are distributed according to multiple type II Matérn hard-core processes. To characterize the blockage process caused by vehicles, a closed-form expression is deduced to distinguish line-of-sight (LOS) and non-LOS transmission. This expression demonstrates that LOS links are independent of horizontal communication distances. Several closed-form probability density functions of the communication distance between a reference platoon and its serving transmitter (other platoons or BSs) are derived for analyzing the generated path loss. After designing three practical user association techniques, tractable expressions for coverage probabilities are figured out. Our work theoretically shows that the maximum density of VPSs exists and large antenna scales benefit the networks' coverage performance. The numerical results illustrate that platoons outperform individual vehicles in terms of road spectral efficiency and the considered system is LOS interference-limited.**

***Index Terms*—Matérn hard-core process, millimeter wave, stochastic geometry, user association techniques, vehicular platoon systems, vehicle-to-everything networks.**

I. Introduction

Compared with traditional sub-6 GHz communications, millimeter-wave (mmWave) systems have smaller data packets, which contributes to ultra-low latencies. Additionally, thanks to the large available spectrum resources, the data rate with mmWave could increase to 7 Gbps [2]. For fast mobile devices, Doppler effects have a non-negligible impact on communication performance. Fortunately, mmWave-enabled antennas are capable to mitigate the Doppler spread via generating high directional beamforming [3]. Benefited by these properties, mmWave communications become popular in modern vehicular networks. This promising research direction has been studied for decades [4–6]. Most initial works focused on the channel measurement and performance evaluation of an individual vehicle in various vehicle-to-infrastructure (V2I) and vehicle-to-vehicle (V2V) scenarios under 5G. In recent LTE Release 15 and beyond, 3GPP investigates the feasibility of enhanced vehicle-to-everything (V2X) communications under, which is fundamental for forthcoming beyond 5G and 6G era [7]. One of the promising user cases is the vehicular platoon system (VPS), where multiple vehicles are grouped into a platoon to share common mobility modes and all participants are controlled by the leading vehicle [8]. This system has attracted increasing attention because of the low traffic congestion [3], high fuel efficiency [9], and comfortable travel experience [10].

A. Related Work and Motivations

For mmWave vehicular communications, the related research can be traced back to 1980s. In 1983, the authors in [4] measured propagation characteristics of two frequencies (35 GHz and 58 GHz) in rail-car-to-infrastructure communications. From 1987 to 1994, a project of European intelligent transportation systems (ITSs) named PROMETHEUS applied 57 GHz into V2V communications [5]. These works indicate that integrating mmWave with V2X communications is able to dramatically enhance the network performance. However, the high cost of mmWave-enabled devices restricted the development of this technology in the early stage [6]. Nowadays, thanks to the advance of integrated circuits used in mmWave bands [11–13], low-cost devices become possible and hence the study on mmWave V2X networks is reinvigorated. Recently, several research efforts have been devoted to exploring such networks [14–17]. During overtaking, the actual V2V propagation channel for the frequency range from 59.75 to 60.25 GHz was measured in [14]. Since vehicular radars are also operated in mmWave bands, the authors in [15] proposed an adaptive cruise control mode to enhance mmWave V2X communications by incorporating radar sensing capabilities. Furthermore, machine learning approaches were introduced in [16] to configure beamforming patterns. Note that the average performance of networks is an important metric for designing new protocols [18]. Although the mentioned results based on measurements or simulations are inspiring, it is not efficient to evaluate the average performance of mmWave V2X networks via the same methods. The main reason is that when considering a large number of transmitters and receivers simultaneously, both the cost and difficulty of experiments are significantly increased. Fortunately, an efficient mathematical tool, namely stochastic geometry, becomes a popular solution

W. Yi, Y. Liu and A. Nallanathan are with Queen Mary University of London, London, UK (email:{w.yi, yuanwei.liu, a.nallanathan}@qmul.ac.uk).

Y. Deng is with King's College London, London, UK (email: yansha.deng@kcl.ac.uk).

R. W. Heath Jr., is with the Department of Electrical and Computer Engineering, The University of Texas at Austin, Austin, TX 78712 USA (email: rheath@utexas.edu).

Part of this work was accepted to be presented in IEEE Global Communications Conference (GLOBECOM), December, Waikoloa, HI, USA, 2019 [1].

due to the strong extensibility and the capability of providing tractable theoretical expressions [19].

For traditional mmWave networks and vehicular communications, stochastic geometry has already been widely utilized [18, 20–27]. The authors in [20] modeled line-of-sight (LOS) and non-LOS (NLOS) base stations (BSs) as two independent thinning Poisson point processes (PPPs) to evaluate the coverage and rate performance of cellular networks. Since mmWave signals are sensitive to obstacles, mmWave communications are frequently applied in short-range networks [21]. To characterize this property, another point process with multiple small cells, namely Poisson cluster processes (PCPs), has been introduced to model the locations of devices in device-to-device (D2D) communications [22] and heterogeneous networks (HetNets) [18]. Regarding the vehicular communications, both roads and vehicles can be modeled with the aid of stochastic geometry. For grid type urban streets, the location of roads are random but the corresponding orientation has only two mutually perpendicular directions. Therefore, an Manhattan Poisson line process (MPLP) is proposed to represent the distribution of this type of roads [23, 28]. To relax the constraint of orientations, the authors in [24] provided another Poisson line process (PLP) model, where both the location and orientation of roads are uniformly distributed. Although the randomness of roads can be captured via PLPs, practical roads decided by the urban planning may hardly follow uniform distributions. For vehicles, PPPs were first used to characterize the distribution of independent vehicles [23, 25]. Then, to depict the traffic congestion at intersections, PCPs were investigated in [26]. It is worth noting that PPPs and PCPs ignore the length of vehicles. This assumption is acceptable for modeling solo-driving scenarios as the length of an individual vehicle is much smaller than communication distances. However, in VPSs, the length of one platoon is non-negligible. To this end, Matérn hard-core process (MHCP) of type II has been investigated in [27]. To simplify the analysis, the authors in [27] regarded MHCP as a stationary thinning PPP, which sacrifices the evaluation accuracy.

Based on the aforementioned discussion, the average coverage evaluation for mmWave V2X networks with VPSs is still in its infancy, which motivates us to contribute this work. More specifically, our paper attempts to solve the following problems:

- **Problem 1:** How to model practical mmWave vehicular networks with VPSs according to MHCPs, especially for blockage processes?
- **Problem 2:** How to derive more accurate distributions of communication distance than existed techniques using an approximated stationary PPP?
- **Problem 3:** What is the best user association technique for one typical platoon to acquire essential information?

B. Contributions

In this paper, we consider a basic traffic element, namely a straight multi-lane road without intersections. One of the lanes contains platoons of autonomous vehicles. We utilize line segments to model platoons and other vehicles with the aid of MHCPs. In addition to V2V communications, road-side units are also included to provide further services. The main contributions are:

- We provide a spatial framework for platoon-based mmWave V2X networks via a PPP and multiple MHCPs. Both V2V and V2I are discussed to enhance the generality. Based on this framework, we deduce a closed-form expression representing the vehicle-caused blockage process. The deduced expression shows that the probability for vehicles being blocked is mainly decided by the number of lanes and the height of blocking vehicles.
- We characterize the distribution of communication distances from a reference platoon to other platoons/road-side units. Closed-form probability density functions (PDFs) for these distances are derived. Under two special cases, namely heavy and light traffic, more efficient PDFs are offered to simplify the analysis.
- We propose three user association techniques, where the typical platoon is able to connect to both platoons and road-side units for supporting various applications. Based on these techniques, theoretical coverage probabilities for a general case are figured out. We further provide several tractable corollaries to discuss the coverage performance under a special case that ignores NLOS transmission. Additionally, we derived closed-form expressions for signal-to-noise (SNR) coverage probabilities.
- We show that 1) compared with the existed approximation PDFs, the proposed PDF of the nearest distance in an MHCP has lower approximation error; 2) without considering the content placement, the typical vehicle achieves the best performance when associating with the transmitter which has the strongest received power; 3) by enlarging the antenna scale, mmWave outperforms sub-6 GHz in terms of both coverage probabilities; 4) platoons have higher road spectral efficiency than traditional individual vehicles; and 5) NLOS transmission and thermal noise have limited impact on the final converge performance.

C. Organization and Notation

The remainder of this article is organized as: Section II introduces the spatial framework with the aid of MHCPs. Section III characterizes different distributions of communication distances. Section IV derives coverage probabilities under three user association techniques. Section V illustrates numerical results. Section VI is our conclusion.

II. System Model

A. Road Model

In this paper, we consider a basic element of the practical road structure, namely a straight one-way road without intersections[1]. This road model can be extended into other complex cases (e.g., two-way roads, roads with intersections,

[1]Note that vehicle models are independent of road models and blockage processes caused by the surrounding environment, e.g, buildings. By introducing other road and blockage models, the proposed framework can be extended into other scenarios.

TABLE I
TABLE OF NOTATION

Symbol	Definition
M, w_l	Number of lanes, width of each lane
n, τ	Number of vehicles in a platoon, length of each vehicle
d_M, d_P	Safety distance for manned vehicles, safety distance for platoons
Φ_p, λ_p	Generating PPP for MHCPs, the corresponding density
Φ_i	MHCP (Distribution of vehicles' receiving antennas in the i-th lane)
$\hat{\Phi}_i$	MHCP (Distribution of vehicles' transmitting antennas in the i-th lane)
λ_i, $\lambda_i^{(2)}$, d_i^h	First order density, second order density, hard core distance of the i-th lane
Φ_{M+1}, λ_{M+1}	PPP, the corresponding density (Distribution of BSs)
H_p, H_b, H_i	Antenna height at PVs, antenna height at BSs, minimal blocking height of MVs in the i-th lane
P_i^H	Ratio of uniformly distributed blocking MVs in the i-th lane
G_m^ϱ, G_s^ϱ, θ_m^ϱ, N_ϱ	Main beam gain, side lobe gain, 3-dB beamwidth, number of antenna elements ($\varrho \in \{v, b\}$)
d_{min}	Minimal communication distance from the typical platoon to its nearest front platoon
C_κ, α_κ	Intercept, path loss exponent ($\kappa \in \{L, N\}$)
P_ϱ, n_0^2	Transmit power, power of thermal noise
$h_{\mathbf{x}}$, N_κ	Small-scale fading term, Nakagami fading parameter
D_1, V_b	Length of a platoon, vertical distance from BSs to the typical platoon
$\mathbb{B}[.]$, $\mathbb{P}[.]$, $\mathbb{E}[.]$	Bernoulli random variable, probability function, expectation function

etc.) via importing angle parameters. The considered road with M lanes is illustrated in Fig. 1 and important parameters are listed in Tab. I. Small BSs are deployed at one side of this road to transmit controlling messages and multimedia content. Platoons of autonomous vehicles (PVs) are driven on the innermost lane and traditional manned vehicles (MVs) are located in the rest $(M-1)$ lanes. The MVs located further than the 1-st lane are ignored as they do not impact on the evaluated performance. For PVs, the leading vehicle controls the following $(n-1)$ participants. Moreover, the separation between two proximate vehicles is larger than the safety distance.

Assumption 1. *The width of vehicles is short and hence it has a negligible impact on the coverage performance. Therefore, vehicles are assumed to be line segments.*

B. Spatial Distributions

We assume the BSs are located in the $(M+1)$-th 'lane' to unify notation. The point process in the i-th lane ($i \in [1, M+1]$) is denoted by Φ_i with density λ_i.

1) Distribution of Base Stations Φ_{M+1}: BSs are distributed as a one-dimensional (1D) PPP with density λ_{M+1}.

2) Distribution of Vehicles $\Phi_i|_{i=1,2,\ldots,M}$: The head of PVs and MVs are modeled by multiple 1D MHCPs. The hard-core distance for MVs is $d_i^h = d_2^h = d_M + \tau$, where $(i \in [2, M])$ and the counterpart for PVs is $d_1^h = n(d_P + \tau)$.

C. Properties of MHCPs

The MHCP is a two-step point process, which is generated from a 1D homogeneous PPP Φ_p with density λ_p. The first step is to associate each point in Φ_p with a uniformly distributed mark m ($m \sim \mathrm{Unif}[0,1]$). The second step is to delete all points if their marks are larger than any point located within the hard-core distance d_h [29]. As a result, the probability that an arbitrary point in Φ_p is retained obeys [30]

$$P_{\mathrm{re}}(d_h) = \int_0^1 \exp(-2m\lambda_p d_h)dm = \frac{1-\exp(-2\lambda_p d_h)}{2\lambda_p d_h}. \quad (1)$$

In our system, by substituting the hard-core distance d_i^h into (1), the first order density λ_i of the MHCP Φ_i can be expressed as

$$\lambda_i = \lambda_p P_{\mathrm{re}}(d_i^h) = \frac{1-\exp(-2\lambda_p d_i^h)}{2d_i^h}, \quad (i \in [1, M]). \quad (2)$$

Remark 1. *The first order density λ_i represents the density of vehicles in the i-th lane. Note that $\lambda_i \leq \frac{1}{2d_i^h}$. If vehicles are randomly distributed, the maximum density of vehicles is $\frac{1}{2d_i^h}$.*

Remark 2. *Since each PV contains n vehicles, the density of vehicles in the 1-st lane equals to $\frac{n(1-\exp(-2\lambda_p d_1^h))}{2d_1^h} = \frac{1-\exp(-2\lambda_p n(\tau+d_P))}{2(\tau+d_P)}$. Therefore, by increasing n, the same road is able to support more vehicles, which means the road capacity is enhanced after considering platoons.*

Since whether a point in an MHCP is retained or not is decided by the conditions of its surrounding points, we need to acquire the second order density for our MHCPs. According to the definition of the second order density [31], when the distance between any two points in Φ_i is r, the corresponding second order density is given by

$$\lambda_i^{(2)}(r) = \mathrm{U}(r-2d_i^h)(\lambda_i^2 - \Omega_i(r)) + (1-\mathrm{U}(d_i^h - r))\Omega_i(r), \quad (3)$$

where

$$\Omega_i(r) = \frac{1-\exp(-2\lambda_p d_i^h)}{d_i^h r} - \frac{2(1-\exp(-\lambda_p(2d_i^h + r))}{r(2d_i^h + r)} \quad (4)$$

and $\mathrm{U}(.)$ is the unit step function which is as follows

$$\mathrm{U}(x) = \begin{cases} 1, & x \geq 0 \\ 0, & x < 0 \end{cases}. \quad (5)$$

D. Directional Beamforming

A typical antenna pattern, namely uniform linear arrays (ULAs) are deployed at PVs and BSs to accomplish directional

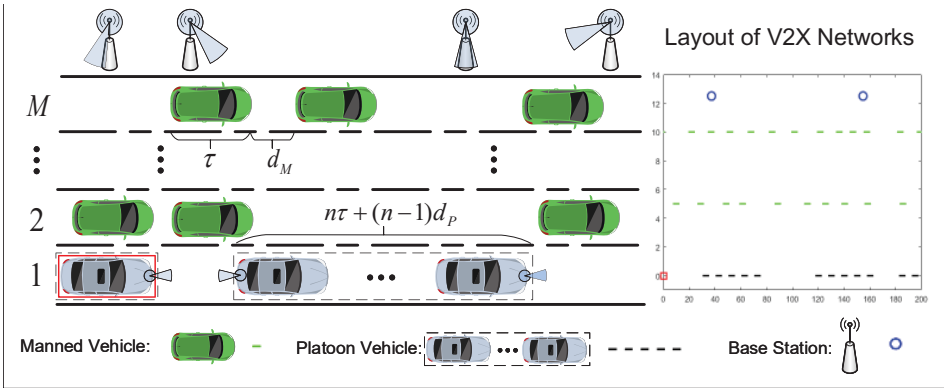

Fig. 1. The layout of proposed mmWave V2X networks with platoons and manned vehicles. For a straight road with multiple lanes, platoons of autonomous vehicles are located in the innermost lane and manned vehicles are driven on the rest lanes of this road. Along the road side, multiple BSs are uniformly distributed. The width of vehicles are ignored and hence all vehicles are modeled with the aid of MHCPs. All BSs are modeled according to a PPP.

beamforming. The number of antenna elements at PVs is N_v and that at BSs is N_b. To simplify the analysis, we utilize a sectorial model with three main antenna parameters to abstractly depict the actual beamforming. These parameters are main beam gain G_m^ϱ, the first side lobe gain G_s^ϱ, and 3-dB beamwidth θ_m^ϱ ($\varrho \in \{v, b\}$). In this system, we consider the ratio of the antenna spacing to the wavelength equals a quarter. Based on the array gain expression in [32], we obtain that $G_m^\varrho = N_\varrho$ and $G_s^\varrho = 1/(N_\varrho \sin^2(3\pi/2N_\varrho))$. By using the cosine antenna pattern in [33], the beamwidth obeys that $\theta_m^\varrho \approx 2\arcsin(2/N_\varrho)$. Compared with other sectorial antenna models in [20, 23], the proposed model has higher accuracy, especially for large antenna scale cases.

For the desired communication link, both the transmitter and receiver should adjust their antenna directions to achieve the maximum array gain $G_m^v G_m^\varrho$. For every interfering link, we assume both the angle of arrival (AoA) and angle of departure (AoD) are uniformly distributed over the range $[0, \pi]$. When the interferer is located at $\mathbf{x}$, the received antenna array gain $G_\mathbf{x}$ for a reference platoon has four values. Each value $a_q^{v\varrho}$ happens with a probability $b_q^{v\varrho}$. The superscript $v\varrho$ means the receiver is a PV and the transmitter is a PV ($\varrho = v$) or a BS ($\varrho = b$). As presented in [20], we summarize all conditions in Tab. II.

TABLE II
VALUES AND PROBABILITIES OF $G_\mathbf{x}$

q	1	2	3	4
$a_q^{v\varrho}$	$G_m^v G_m^\varrho$	$G_s^v G_m^\varrho$	$G_m^v G_s^\varrho$	$G_s^v G_s^\varrho$
$b_q^{v\varrho}$	$\frac{\theta_m^v}{\pi}\frac{\theta_m^\varrho}{\pi}$	$(1-\frac{\theta_m^v}{\pi})\frac{\theta_m^\varrho}{\pi}$	$\frac{\theta_m^v}{\pi}(1-\frac{\theta_m^\varrho}{\pi})$	$(1-\frac{\theta_m^v}{\pi})(1-\frac{\theta_m^\varrho}{\pi})$

Assumption 2. *Compared with PVs, MVs have fewer requirements of communications as most actions are decided by the driver rather than vehicular networks. We assume MVs use traditional sub-6 GHz to communicate with other devices. Since we focus on the performance of PVs, the antenna deployment of MVs are omitted in this paper.*

Assumption 3. *In practice, the antenna can be deployed at different positions, e.g., the top of vehicles [34], the headlight of vehicles [35], etc. In this paper, we assume that two antennas are separately deployed at the front and rear headlight of a vehicle. The front antenna is used for receiving messages and the rear antenna is in charge of transmitting information. This scenario is a general case including complete blockage and path loss models. By modifying some parameters (e.g., vehicle height, the distance between two antennas, etc.), the considered scenario can be changed to other cases with different antenna deployment. Moreover, due to knowing the transmitted information, the self-interference between these two antennas can be compensated.*

Assumption 4. *We ignore Doppler effects. The reason is that the angular spread in mmWave communications with high directional beamforming is relatively small [36]. Moreover, Doppler effects can be further compensated by applying automatic frequency control loops [37].*

E. Blockage Model

In this part, we discuss the blockage effects caused by vehicles. In the i-th lane ($i \geq 2$), blocking MVs with a height higher than the minimum blocking height H_i are capable of obstructing the LOS transmission between BSs and PVs. As shown in Fig. 2, since the length ratios of two similar triangles are equal, we obtain that $H_i = \frac{2(i-1)H_b+(2M-2i+1)H_p}{2M-1}$. In reality, the heights of MVs are different, so we assume in the i-th lane, the ratio of uniformly distributed blocking MVs is P_i^H. As a result, the first order density of blocking MVs is $P_i^H \lambda_i$.

Lemma 1. *For V2I scenarios, when one BS communicates with the considered PV and the height of the i-th lane's MVs in excess of H_i has a probability P_i^H, the probability $P_L(M)$ for the BS not being blocked is given by*

$$P_L(M) = \prod_{i=1}^{\max(M-1,1)} (\mathrm{U}(M-1) - P_i^H \lambda_i \tau \mathrm{U}(M-2)), \quad (6)$$

Proof: See Appendix A. ∎

For V2V communications in the 1-st lane, only adjacent PVs have LOS links. We use $M = 0$ to represent this case. Therefore, $P_L(0) = \mathrm{U}(d_{min})$. It is intuitive that the probability

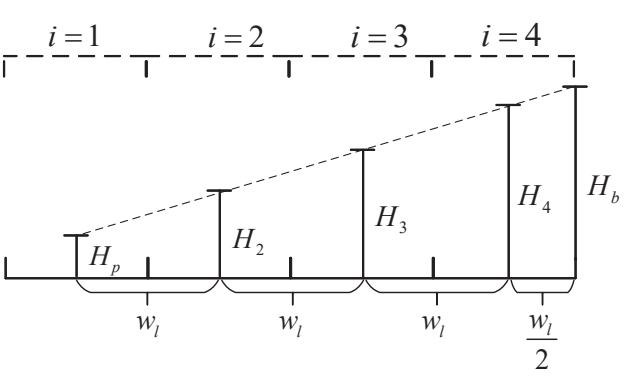

Fig. 2. A four-lane example ($M = 4$) to illustrate the minimum blocking height H_i in the i-th lane with the height of antenna at PVs H_p and at BSs H_b.

of experiencing NLOS links is $P_N(M) = 1 - P_L(M)$. Therefore, the corresponding path loss law can be expressed as follows

$$\mathrm{L}(M, r) = \mathbb{B}\left[P_L(M)\right] C_L r^{-\alpha_L} + \mathbb{B}\left[P_N(M)\right] C_N r^{-\alpha_N}, \quad (7)$$

where $\mathbb{B}[p]$ is a Bernoulli random variable with the parameter of success probability p. The C_κ is the intercept and α_κ represents the path loss exponent. The notation $\kappa = L$ means LOS transmission and $\kappa = N$ means NLOS scenarios.

Assumption 5. *To achieve fast responses for internal vehicles of PVs, we assume that the internal communications of PVs use different wireless transmission techniques, e.g., visible light communications [35], to avoid mutual interference with outside mmWave communications.*

F. Signal Model

In our V2X networks, one randomly selected PV is *the typical PV*. Since the locations of receiving antennas are modeled by Φ_1 and two antennas in one PV separates with a constant distance $D_1 = d_1^h - d_P$, the locations of transmitting antennas can be modeled by the same point process but with different locations. We assume the set of transmitting antenna locations is $\hat{\Phi}_1$. More specifically, every point $\mathbf{x} \in \Phi_1$ has a corresponding point $\hat{\mathbf{x}} \in \hat{\Phi}_1$ and they obeys

$$\|\mathbf{x} - \hat{\mathbf{x}}\| = D_1, \quad \forall\, \mathbf{x} \in \Phi_1. \quad (8)$$

We assume the typical PV is located at the origin, namely $\mathbf{x}_0 = (0, 0) \in \Phi_1$. When the typical PV connects with another PV that has a transmitting antenna at $\hat{\mathbf{x}}_s \in \hat{\Phi}_1$, the received SINR is denoted by $\Upsilon_{\hat{\mathbf{x}}_s}$. When it turns to a BS at $\mathbf{x}_b \in \Phi_{M+1}$, the received SINR is $\Upsilon_{\mathbf{x}_b}$. As a result, two kinds of SINR are shown at the top of next page, where $h_{\mathbf{x}}$ is a small-scale fading term for one communication channel with a transmitter at $\mathbf{x}$. We adopt Nakagami fading channels with parameter N_κ. Therefore, $|h_{\mathbf{x}}|^2$ is a Gamma variable [22].

III. Distance Distribution in Multi-MHCPs

In this section, we focus on the distributions of different distances. Since the typical PV is able to acquire information from both PVs and BSs, there exist three kinds of distances: a) the distance to the nearest PV; b) the distance to the BS that provides the strongest received power at the typical PV; and c) the distance to the transmitter (BS or PV) with the strongest received power. In the following content, we discuss them separately.

A. Distance to Nearest PV

Note that all receiving antennas of PVs are modeled with the MHCP Φ_1 and the typical vehicle is located at the origin $\mathbf{x}_0 = (0, 0)$. In the 1-st lane, assuming the nearest point to $\mathbf{x}_0$ is $\mathbf{x}_s \in \Phi_1$. The process of $\mathbf{x}_s$ can be regarded as a thinning process of its generating PPP Φ_p. The corresponding thinning probability is presented in the following lemma.

Lemma 2. *In the MHCP Φ_1, the thinning probability $\rho_1(r_s)$ for the nearest point $\mathbf{x}_s$ is conditional on the nearest distance $r_s = \|\mathbf{x}_s\|$, which is given by*

$$\rho_1(r_s) \approx \begin{cases} \frac{f_n(2d_1^h, d_1^h) + f_n(3d_1^h - r_s, r_s)}{P_{\mathrm{re}}(d_1^h)} \mathrm{U}(r_s - d_1^h), & r_s < 2d_1^h \\ C_1 = \frac{f_n\left(2d_1^h, d_1^h\right) + f_n\left(d_1^h, 2d_1^h\right)}{P_{\mathrm{re}}(d_1^h)}, & r_s \geq 2d_1^h, \end{cases} \quad (11)$$

where

$$f_n(a, b) = \frac{1 - \exp(-\lambda_p a)}{\lambda_p^2 ab} - \frac{1 - \exp(-\lambda_p (a + b))}{\lambda_p^2 (a + b) b}. \quad (12)$$

Proof: See Appendix B. ∎

Proposition 1. *Based on* **Lemma 2***, the closed-form PDF of the nearest distance r_s is*

$$f_{\rho_1}(r_s) \approx \begin{cases} \frac{\lambda_p (f_n(2d_1^h, d_1^h) + f_n(3d_1^h - r_s, r_s))}{P_{\mathrm{re}}(d_1^h)} \\ \quad \times \exp\left(-\frac{\lambda_p \left(\Psi(r_s) - \Psi\left(d_1^h\right)\right)}{P_{\mathrm{re}}(d_1^h)} \right) \mathrm{U}(r_s - d_1^h), & r_s < 2d_1^h \\ \lambda_p C_1 \exp\left(-\lambda_p \left(C_2 + C_1 (r_s - 2d_1^h)\right)\right), & r_s \geq 2d_1^h, \end{cases} \quad (13)$$

where

$$\Psi(x) = f_n(2d_1^h, d_1^h) x + \frac{\mathrm{Ei}\left(-\lambda_{\mathrm{p}}(3\mathrm{d}_1^{\mathrm{h}} - \mathrm{x})\right) - \ln(\mathrm{x} - 3\mathrm{d}_1^{\mathrm{h}})}{3d_1^h \lambda_p^2} - \frac{\exp\left(-3\lambda_p d_1^h\right) \left(\mathrm{Ei}\left(\lambda_{\mathrm{p}} \mathrm{x}\right) - \ln(\mathrm{x})\right)}{3d_1^h \lambda_p^2} \quad (14)$$

$$\Upsilon_{\hat{\mathbf{x}}_s}=\frac{\mathcal{P}_v \mathrm{L}\left(0,\|\hat{\mathbf{x}}_s\|\right) G_m^v G_m^v |h_{\hat{\mathbf{x}}_s}|^2}{\sum\limits_{\hat{\mathbf{x}}\in\hat{\Phi}_1\setminus\hat{\mathbf{x}}_0,\hat{\mathbf{x}}_s}\mathcal{P}_v \mathrm{L}\left(0,\|\hat{\mathbf{x}}\|\right) G_{\hat{\mathbf{x}}}|h_{\hat{\mathbf{x}}}|^2+\sum\limits_{\mathbf{x}\in\Phi_{M+1}}\mathcal{P}_b \mathrm{L}\left(M,\|\mathbf{x}\|\right) G_{\mathbf{x}}|h_{\mathbf{x}}|^2+n_0^2}, \tag{9}$$

$$\Upsilon_{\mathbf{x}_b}=\frac{\mathcal{P}_b \mathrm{L}\left(M,\|\mathbf{x}_b\|\right) G_m^v G_m^b |h_{\mathbf{x}_b}|^2}{\sum\limits_{\hat{\mathbf{x}}\in\hat{\Phi}_1\setminus\hat{\mathbf{x}}_0}\mathcal{P}_v \mathrm{L}\left(0,\|\hat{\mathbf{x}}\|\right) G_{\hat{\mathbf{x}}}|h_{\hat{\mathbf{x}}}|^2+\sum\limits_{\mathbf{x}\in\Phi_{M+1}\setminus\mathbf{x}_b}\mathcal{P}_b \mathrm{L}\left(M,\|\mathbf{x}\|\right) G_{\mathbf{x}}|h_{\mathbf{x}}|^2+n_0^2}. \tag{10}$$

and the constant $C_2=\int_{d_1^h}^{2d_1^h}\rho_1(r_s)dr_s$, $\mathrm{Ei(x)}$ is the exponential integral.

Proof: Based on this thinning process, the cumulative distribution function (CDF) of the nearest point r_s is given by [31]

$$F_{\rho_1}(r_s)=1-\exp\left(-\lambda_p\int_0^{r_s}\rho_1(t)dt\right). \tag{15}$$

Then the PDF of the distance r_s can be expressed as

$$f_{\rho_1}(r_s)=\frac{dF_{\rho_1}(r_s)}{dr_s}=\lambda_p\rho_1(r_s)\exp\left(-\lambda_p\int_0^{r_s}\rho_1(t)dt\right). \tag{16}$$

Note that one typical integral is $\int\frac{1-\exp(c-at)}{t(b-t)}dt=\frac{\exp(c-ab)\mathrm{Ei(a(b-x))}-\exp(c)\mathrm{Ei}(-\mathrm{ax})-\log(1-\mathrm{b/x})}{b}+\text{constant}$. *By substituting* (11) *into* (16)*, we have this proposition.* ∎

Remark 3. *Since we regard the probability $\mathbb{P}[\Phi_p\cap l_3=\emptyset]$ as $\mathbb{P}[\Phi_1\cap l_3=\emptyset]$ in* (B.2)*, a few MHCP points located in l_3 have been ignored. Therefore, the proposed PDF is a lower bound of exact results. With the increase of l_3, the accuracy of* **Proposition 1** *degrades. However, this degradation has limited impact on coverage performance as long communication distances, namely large l_3, have severe path loss, which results in the relatively small received power.*

Although **Proposition 1** provides a closed-form expression, it is inefficient to calculate the integral of $\mathrm{Ei(x)}$. Therefore, we further simplified this PDF based on two practical scenarios, namely *light traffic* and *heavy traffic*.

Corollary 1. *For the light traffic, the generating density λ_p should be small. Then the PDF of the nearest distance r_s is given by*

$$\ddot{f}_{\rho_1}(r_s)\approx\lambda_p\exp(-\lambda_p(r_s-d_1^h)). \tag{17}$$

Proof: When $\lambda_p d_1^h\to 0$, $P_{\mathrm{re}}(d_1^h)\to 1$. *In other words, almost all points in the generating PPP are retained. Therefore, the MHCP Φ_1 can be regraded as the generating PPP Φ_p. With the aid of the PDF for the nearest distance in a PPP [18], we have this corollary.* ∎

Since PPP-based models for mmWave vehicular networks have been analyzed in various papers [23, 25], we omit the analysis for the light traffic scenario in the rest of this work.

Corollary 2. *For the heavy traffic, the generating density λ_p should be large. Then the PDF of the nearest distance r_s is at the top of next page.*

Proof: Note that $\exp(-x)$ converges faster than $\frac{1}{x}$. For $\lambda_p x>2$, $\frac{1-\exp(-\lambda_p x)}{\lambda_p x}\approx\frac{1}{\lambda_p x}$. We substitute $f_n(a,b)\approx\frac{1}{\lambda_p^2 a(a+b)}$ and $P_{\mathrm{re}}(d_1^h)=\frac{1}{2\lambda_p d_1^h}$ *into* **Proposition 1** *to have this corollary.* ∎

Remark 4. *Under the heavy traffic, the PDF of the nearest distance $\dot{f}_{\rho_1}(r_s)$ is independent of λ_p, namely the generating PPP. Moreover, $\dot{f}_{\rho_1}(.)$ is the upper limit of $f_{\rho_1}(.)$ in terms of λ_p.*

Remark 5. *For any d_1^h, the probability that the nearest PV located in the range $(r<2d_1^h)$ is a constant $(1-\exp(-\frac{1+2\ln 2}{3}))\approx 55\%$.*

Corollary 3. *For the heavy traffic, when $d_1^h<r_s<2d_1^h$, The PDF $\dot{f}_{\rho_1}(r_s)$ has a tight lower bound, which is given by*

$$\dot{f}_{\rho_1}(r_s)>\exp\left(\frac{1-\ln(3d_1^h)-2\ln(2d_1^h)}{3}\right)\times\frac{5d_1^h-r_s}{3d_1^h}\exp\left(-\frac{2r_s}{9d_1^h}\right). \tag{19}$$

Proof: Note that $\ln(1+x)<x$ when $(|x|<1)$. *By applying this fact into* **Corollary 2***, we obtain this corollary.* ∎

It is worth noting that the transmitting antenna for the PV at $\mathbf{x}_s$ is located at $\hat{\mathbf{x}}_s\in\hat{\Phi}_1$. Therefore the corresponding communication distance is $\hat{r}_s=\|\hat{\mathbf{x}}_s\|=r_s-D_1$.

Corollary 4. *In the 1-st lane, when the typical vehicle at $\mathbf{x}_0$ communicates with the nearest intra-lane PV at $\mathbf{x}_s$, the communication distance is $\hat{r}_s=\|\hat{\mathbf{x}}_s\|=r_s-D_1>d_P$. Then, the PDF of this distance can be expressed as*

$$f_v(\hat{r}_s)=f_{\rho_1}(\hat{r}_s+D_1). \tag{20}$$

Proof: By substituting $r_s=\hat{r}_s+D_1$ into (11)*, we have this corollary.* ∎

In the **Corollary 4**, the considered expression $f_{\rho_1}(.)$ can be changed to $\dot{f}_{\rho_1}(.)$ and $\ddot{f}_{\rho_1}(.)$. The comparison of these PDFs is provided in the numerical results part.

B. Distance to Desired BS

In this case, the typical PV should associate with the BS having the strongest received power. It is decided by both the communication distance and channel status. Therefore, the PDF of nearest distance can be divided into LOS and NLOS scenarios. The vertical distance from the typical PV to the $(M+1)$-th lane is denoted by $V_b=(M-\frac{1}{2})w_l$.

Lemma 3. *When the desired BS in the $(M+1)$-th lane is located at $\mathbf{x}_b\in\Phi_{M+1}$, the communication distance is $\hat{r}_b=$*

$$\dot{f}_{\rho_1}(r_s) \approx \begin{cases} \frac{5d_1^h - r_s}{3d_1^h} \exp\left(-\frac{r_s - d_1^h}{3d_1^h} - \frac{1}{3}\ln(3d_1^h - r_s) - \frac{2}{3}\ln(2d_1^h)\right) \mathrm{U}(r_s - d_1^h), & r_s < 2d_1^h \\ \frac{\exp((5-2\ln 2)/3)}{d_1^h} \exp\left(-\frac{r_s}{d_1^h}\right), & r_s \geq 2d_1^h \end{cases}. \tag{18}$$

$\|\mathbf{x}_b\| \geq V_b$. *The PDFs for the typical PV associating with a LOS BS* $f_b^L(\hat{r}_b)$ *or a NLOS BS* $f_b^N(\hat{r}_b)$ *are given by*

$$f_b^L(\hat{r}_b) = \begin{cases} \frac{\lambda_b^L \hat{r}_b}{\sqrt{\hat{r}_b^2 - V_b^2}} \exp\left(-\lambda_b^L \sqrt{\hat{r}_b^2 - V_b^2}\right) \\ \times \mathrm{U}(\hat{r}_b - V_b), & \hat{r}_b < \Pi_{\mathrm{th}} \\ \frac{\lambda_b^L \hat{r}_b}{\sqrt{\hat{r}_b^2 - V_b^2}} \exp\left(-\lambda_b^L \sqrt{\hat{r}_b^2 - V_b^2}\right. \\ \left.-\lambda_b^N \sqrt{\Pi_L^2(\hat{r}_b) - V_b^2}\right), & \hat{r}_b \geq \Pi_{\mathrm{th}}, \end{cases} \tag{21}$$

$$f_b^N(\hat{r}_b) = \frac{\lambda_b^N \hat{r}_b}{\sqrt{\hat{r}_b^2 - V_b^2}} \exp\left(-\lambda_b^N \sqrt{\hat{r}_b^2 - V_b^2}\right. \\ \left.-\lambda_b^L \sqrt{\Pi_N^2(\hat{r}_b - V_b^2)}\right) \mathrm{U}(\hat{r}_b - V_b), \tag{22}$$

where $\lambda_b^\kappa = \lambda_b P_\kappa(M)$, $\Pi_L(x) = (C_N x^{\alpha_L}/C_L)^{1/\alpha_N}$, $\Pi_{\mathrm{th}} = \sqrt[\alpha_L]{(C_L/C_N) V_b^{\alpha_N}}$, *and* $\Pi_N(x) = (C_L x^{\alpha_N}/C_N)^{1/\alpha_L}$.

Proof: See Appendix C. ∎

C. Distance to Desired Transmitter

Unlike the previous two cases, when the typical PV connects to the BS or PV with the strongest received power, the PDF of the corresponding distance should consider the channel conditions at both PVs and BSs.

Lemma 4. *If the nearest PV at* $\hat{\mathbf{x}}_s \in \hat{\Phi}_1$ *has stronger received power at the typical PV than all BSs, the communication distance obeys* $\hat{r}_t = \|\hat{\mathbf{x}}_s\| > d_P$. *Then the PDF for the typical PV associating with the nearest PV can be expressed as*

$$f_t^v(\hat{r}_t) \approx \begin{cases} f_v(\hat{r}_t), & \hat{r}_t \leq \frac{V_b}{C_3^L} \\ \exp\left(-\lambda_b^L \sqrt{\left(C_3^L \hat{r}_t\right)^2 - V_b^2}\right) f_v(\hat{r}_t), & \frac{V_b}{C_3^L} < \hat{r}_t \leq \frac{\Pi_{\mathrm{th}}}{C_3^L} \\ \left(\int_{C_3^L \hat{r}_t}^{\infty} f_b^L(x)dx \right. \\ \left. + \int_{C_3^N \Pi_L(\hat{r}_t)}^{\infty} f_b^N(x)\,dx\right) f_v(\hat{r}_t), & \hat{r}_t > \frac{\Pi_{\mathrm{th}}}{C_3^L}, \end{cases} \tag{23}$$

where $C_3^\kappa = (N_b \mathcal{P}_b / N_v \mathcal{P}_v)^{1/\alpha_\kappa}$.

Proof: For the PV scenario, the PDF of the communication distance is defined as

$$\begin{aligned} & f_t^v(\hat{r}_t) \\ =& \mathbb{P}[a_1^{vv}\mathcal{P}_v C_L \hat{r}_t^{-\alpha_L} \geq \max(a_1^{vb}\mathcal{P}_b C_L r_L^{-\alpha_L}, a_1^{vb}\mathcal{P}_b C_N r_N^{-\alpha_N})] \\ =& \mathbb{P}\left[r_L \geq C_3^L \hat{r}_t, C_L r_L^{-\alpha_L} \geq C_N r_N^{-\alpha_N}\right] \\ & + \mathbb{P}\left[r_N \geq C_3^N \Pi_L(\hat{r}_t), C_N r_N^{-\alpha_N} \geq C_L r_L^{-\alpha_L}\right], \end{aligned} \tag{24}$$

where r_L *is the distance to the nearest LOS and* r_N *is the distance to the nearest NLOS BS. With the similar proof procedure in* **Lemma 3***, we are able to derive the analytical expressions for* (24). ∎

Lemma 5. *If one BS at* $\mathbf{x}_b \in \Phi_{M+1}$ *has the strongest received power at the typical PV, the communication distance changes to* $\hat{r}_t = \|\hat{\mathbf{x}}_b\| > V_b$. *The PDFs for the typical PV associating with a LOS BS* $f_t^L(\hat{r}_t)$ *or a NLOS BS* $f_t^N(\hat{r}_t)$ *are given by*

$$f_t^L(\hat{r}_t) \approx \left(1 - \int_{d_P}^{\hat{r}_t/C_3^L} f_v(x)dx\right) f_b^L(\hat{r}_t), \tag{25}$$

$$f_t^N(\hat{r}_t) \approx \left(1 - \int_{d_P}^{\Pi_N(\hat{r}_t)/C_3^L} f_v(x)dx\right) f_b^N(\hat{r}_t). \tag{26}$$

Proof: For BS scenarios, the PDFs of the communication distance when the typical PV connecting with a LOS BS or a NLOS BS are defined as

$$f_t^L(\hat{r}_t) = \mathbb{P}\left[\hat{r}_s \geq \hat{r}_t/C_3^L, C_L \hat{r}_t^{-\alpha_L} \geq C_N r_N^{-\alpha_N}\right], \tag{27}$$

$$f_t^N(\hat{r}_t) = \mathbb{P}\left[\hat{r}_s \geq \hat{r}_t/C_3^N, C_L r_L^{-\alpha_L} < C_N \hat{r}_t^{-\alpha_N}\right]. \tag{28}$$

By applying the similar proof with **Lemma 4***, we obtain this lemma.* ∎

When calculating the PDF expressions in **Lemma 4** and **5**, there is a precondition that for PV scenarios the $\hat{r}_t$ should be larger than d_P and for BS cases the $\hat{r}_t$ should be larger than V_b.

IV. Coverage Performance in V2X Networks

In this section, we propose three user association techniques: a) nearest PV (NP) technique, where the typical PV connects with the nearest intra-lane PV in front of it; b) strongest BS (SB) technique, where the typical PV communicates with the BS which has the strongest received power; and c) strongest transmitter (ST) technique, where the typical PV connects to the PV or BS with the strongest received power.

A. Nearest PV Technique

In V2V networks, autonomous vehicles frequently request both control information and front-road information from the vehicle in front before process any actions. Therefore, the performance of such scenario is important. Before deriving the coverage probability, we first evaluate the impact of interference with the aid of Laplace transform.

1) Laplace Transform of Interference: When the typical PV communicates with the nearest PV, the conditional Laplace transform of interference can be presented in the following lemma.

Proposition 2. *Note that the transmitting antenna of the nearest PV is located at* $\hat{\mathbf{x}}_s \in \hat{\Phi}_1$. *The communication distance between the typical PV and its nearest front PV is* $\hat{r}_s = \|\hat{\mathbf{x}}_s\|$. *Under the NP technique, the Laplace transform of interference*

is conditional on $\hat{r}_s$, which can be expressed as follows

$$\mathcal{L}_{\mathrm{NP}}\left(s\left|\hat{r}_s\right.\right) \approx \prod_{q=1}^{4} \mathcal{L}_{V_L}^{q}\left(s\right) \mathcal{L}_{V_N}^{q}\left(s\right) \times \exp\left(-\frac{s\mathcal{P}_v C_N \bar{G}_{vv}}{\lambda_1} \int_{d_1^h}^{\infty} \lambda_1^{(2)}\left(u\right)\left(u+\hat{r}_1\right) du\right), \quad (29)$$

where the $\bar{G}_{v\varrho}$ is the expectation of antenna gain and it equals to $\sum_{q=1}^{4} a_q^{v\varrho} b_q^{v\varrho}$. Moreover, the LOS ($\kappa = L$) and NLOS ($\kappa = N$) part for the interference from BSs is given by

$$\mathcal{L}_{V_\kappa}^{q}\left(s\right) = \exp\Bigg(- \lambda_b P_\kappa\left(M\right) b_q^{vb} \int_0^{\infty} \Big(1 - \left(1 + \frac{s\mathcal{P}_b C_\kappa a_q^{vb}}{N_\kappa\left(u^2+V_b^2\right)^{\frac{\alpha_\kappa}{2}}}\right)^{-N_\kappa}\Big) du\Bigg). \quad (30)$$

Proof: See Appendix D. ∎

Compared with LOS interference in numerous mmWave networks [18, 20, 22], NLOS interference has a negligible impact on the coverage performance. Additionally, the path loss law for LOS links is similar to free space transmission, namely $\alpha_L \approx 2$. To simplify the analytical expressions, we propose a special case as follows:

Special Case: NLOS transmission is ignored and the path loss exponent obeys $\alpha_L = 2$.

Corollary 5. *Under the special case, the closed-form Laplace transform of the interference under the NP technique is*

$$\tilde{\mathcal{L}}_{\mathrm{NP}}\left(s\right) = \prod_{q=1}^{4} \exp\left(-\lambda_b P_L\left(M\right) b_q^{vb} g_{\mathrm{NP}}^{q}\left(s\right)\right), \quad (31)$$

where

$$g_{\mathrm{NP}}^{q}\left(s\right) = \sum_{j=1}^{N_L} \binom{N_L}{j} (-1)^{j+1} \left(\frac{s\mathcal{P}_b C_L a_q^{vb}}{N_L}\right)^{j} \times \frac{\Gamma\left(1/2\right)\Gamma\left(j-1/2\right)}{2\Gamma\left(j\right)} \left(\mathrm{Z}_q\left(s\right)\right)^{\frac{1}{2}-j} \quad (32)$$

and $\mathrm{Z}_q\left(s\right) = s\mathcal{P}_b C_L a_q^{vb}/N_L + V_b^2$. $\Gamma(x)$ is the Gamma function.

Proof: By deleting the NLOS parts from **Proposition 2** *and then applying a typical integral (4.11) in [38] that is*

$$\int_0^{\infty} \left(x^2+d\right)^{-j} dx = \frac{\Gamma\left(1/2\right)\Gamma\left(j-1/2\right)}{\Gamma\left(j\right)} \frac{\sqrt{d}}{2d^j}, \quad (33)$$

we obtain this expression under the special case. ∎

2) Coverage Probability: The coverage probability is the probability for the received SINR exceeding a threshold Υ_{th}. Therefore, in the NP technique, the coverage probability is

$$P_{\mathrm{NP}}\left(\Upsilon_{th}\right) = \mathbb{P}\left[\Upsilon_{\hat{\mathbf{x}}_s} > \Upsilon_{th}\right]. \quad (34)$$

Theorem 1. *Under the NP technique, the coverage probability at the typical PV with a SINR threshold Υ_{th} is given by*

$$P_{\mathrm{NP}}\left(\Upsilon_{th}\right) \approx \sum_{k=1}^{N_L} (-1)^{k+1} \binom{N_L}{k} \int_{d_P}^{\infty} \exp\left(-kS_v^L\left(\hat{r}_s\right) n_0^2\right) \times \mathcal{L}_{\mathrm{NP}}\left(kS_v^L\left(\hat{r}_s\right)|\hat{r}_s\right) f_v\left(\hat{r}_s\right) d\hat{r}_s, \quad (35)$$

where $S_v^\kappa(\hat{r}_s) = \frac{\eta_\kappa \Upsilon_{th} \hat{r}_s^{\alpha_\kappa}}{\mathcal{P}_v G_m^v G_m^v C_\kappa}$ and $\eta_\kappa = N_\kappa (N_\kappa!)^{-1/N_\kappa}$.

Proof: The proof procedure is similar with Appendix C in [20]. It is worth noting that the desired transmission between the typical PV and its nearest PV is always LOS. ∎

Corollary 6. *Under the special case, a more efficient expression than* **Theorem 1** *is as follows*

$$\tilde{P}_{\mathrm{NP}}\left(\Upsilon_{th}\right) \approx \sum_{k=1}^{N_L} (-1)^{k+1} \binom{N_L}{k} \int_{d_P}^{\infty} \exp\left(-kS_v^L\left(\hat{r}_s\right) n_0^2\right) \times \tilde{\mathcal{L}}_{\mathrm{NP}}\left(kS_v^L\left(\hat{r}_s\right)\right) f_v\left(\hat{r}_s\right) d\hat{r}_s, \quad (36)$$

Proof: By replacing $\mathcal{L}_{\mathrm{NP}}(.)$ with $\tilde{\mathcal{L}}_{\mathrm{NP}}(.)$, we have this corollary. ∎

Remark 6. *Note that $\tilde{\mathcal{L}}_{\mathrm{NP}}\left(kS_v^L a\left(\hat{r}_s\right)\right)$ has a negative correlation with $P_L(M)$. Therefore, the coverage probability under the NP technique is a monotonic increasing function with the number of lanes M. For roads with large M, the proposed network under the NP technique is a noise-limited system because $P_L(M) \to 0 \Rightarrow \tilde{\mathcal{L}}_{\mathrm{NP}}\left(kS_v^L a\left(\hat{r}_s\right)\right) \to 1$.*

Since modern networks have various interference cancellation techniques, SNR is also important. When considering the SNR coverage probability under the heavy traffic, we provide a closed-form lower bound in the following part.

Corollary 7. *For the heavy traffic, a closed-form lower bound for SNR coverage probability under the special case can be expressed as*

$$\ddot{P}_{\mathrm{NP}}\left(\Upsilon_{th}\right) > \sum_{k=1}^{N_L} (-1)^{k+1} \binom{N_L}{k} C_5\Big(f_{\mathrm{NP}}\left(C_4, C_6, 4d_1^h\right) - f_{\mathrm{NP}}(C_4, C_6, 3d_1^h)\Big) + \frac{1}{2d_1^h} \exp\big(\frac{5-2\ln 2)}{3} - \frac{D_1}{d_1^h}\big) \sqrt{\frac{\pi}{C_4}} \times \exp\big(\frac{1}{4C_4 (d_1^h)^2}\big)\big(1 - \mathrm{erf}\big(\frac{1}{2d_1^h}\sqrt{\frac{1}{C_4}} + \sqrt{C_4}(d_P + d_1^h)\big)\big)\Big), \quad (37)$$

where $f_{\mathrm{NP}}\left(a,b,t\right) = \frac{\sqrt{\pi} b \exp\left(b^2/4a\right)}{4a^{3/2}} \mathrm{erf}\left(\frac{2at-b}{2\sqrt{a}}\right) - \frac{\exp\left(-at^2+bt\right)}{2a}$, $C_4(\Upsilon_{th}) = \frac{k\eta_L \Upsilon_{th} n_0^2}{\mathcal{P}_v G_m^v G_m^v C_L}$, $C_5(\Upsilon_{th}) = \frac{1}{3d_1^h} \exp\big(-\frac{3\ln\left(3d_1^h\right)+6\ln\left(2d_1^h\right)+7}{9} - C_4\left(5d_1^h - D_1\right)^2\big)$, and $C_6(\Upsilon_{th}) = C_4(\Upsilon_{th})\left(5d_1^h - D_1\right) + \frac{2}{9d_1^h}$. The $\mathrm{erf}(.)$ is the error function. To save the space, the variable notation (Υ_{th}) is omitted here.

Proof: By deleting the interference part $\mathcal{L}_{\mathrm{NP}}(.)$ and substituting **Corollary 3** *in* **Corollary 6**, *we have this corollary.* ∎

Remark 7. *Based on* **Remark 4**, *the coverage performance of the heavy traffic under the NP technique is independent on the generating PPP's density λ_p, which means the density of PVs in the 1-st lane can be regarded as $\frac{1}{2d_1^h}$ under this scenario.*

B. Strongest BS Technique

In addition to requesting sensing information from the nearest PV, the typical PV also need to download large data

packages, e.g. high resolution on-line maps, high-definition movies, cloud-based controlling information, etc. The content is better to be acquired from a BS that connect with the core server rather than other vehicles. Therefore, the performance of associating with the strongest BS is also an important case.

1) Laplace Transform of Interference: When the typical PV requires messages from BSs, the conditional Laplace transform of interference is provided in the following lemma.

Proposition 3. *Under the SB technique, the location of the desired BS is $\mathbf{x}_b$ and the communication distance is $\hat{r}_b = \|\mathbf{x}_b\|$. After that, the Laplace transform of interference is conditional on $\hat{r}_b$, which is given by*

$$\mathcal{L}_{\mathrm{SB}}\left(s\,|\hat{r}_b\,\right) \approx \prod_{q=1}^{4} \mathcal{L}^{q}_{B_L}\left(s|\hat{r}_b\right) \mathcal{L}^{q}_{B_N}\left(s|\hat{r}_b\right) \exp\left(-\frac{s\mathcal{P}_v C_N \bar{G}_{vv}}{\lambda_1} \int_{d_1^h}^{\infty} \lambda_1^{(2)}\left(u\right)\left(u\right) du\right), \tag{38}$$

where

$$\mathcal{L}^{q}_{B_\kappa}\left(s|\hat{r}_b\right) = \exp\Bigg(-\lambda_b^{\kappa}\left(M\right) b_q^{vb} \int_{\Xi_\kappa}^{\infty} \Bigg(1 - \left(1 + \frac{s\mathcal{P}_b C_\kappa a_q^{vb}}{N_\kappa\left(u^2+V_b^2\right)^{\frac{\alpha_\kappa}{2}}}\right)^{-N_\kappa}\Bigg) du\Bigg) \tag{39}$$

and Ξ_κ is defined as follows: 1) when the desired transmission between the typical PV and the serving BS is LOS, $\Xi_L = \hat{r}_b$ and $\Xi_N = \Pi_L(\hat{r}_b)$; and 2) when the desired transmission is NLOS, $\Xi_L = \Pi_N(\hat{r}_b)$ and $\Xi_N = \hat{r}_b$.

Proof: The proof is similar with **Proposition 2** *and we omit it here.* ∎

Corollary 8. *Under the special case, the tractable Laplace transform of the interference with the SB technique can be expressed as*

$$\tilde{\mathcal{L}}_{\mathrm{SB}}\left(s|\hat{r}_b\right) \approx \prod_{q=1}^{4} \exp\left(-\lambda_b^L b_q^{vb} g^{q}_{\mathrm{SB}}\left(s|\hat{r}_b\right)\right) \int_{d_P}^{\infty} \sum_{q'=1}^{4} b_{q'}^{vv}\left(1 + \frac{s\mathcal{P}_v C_L a_{q'}^{vv}}{N_L \hat{r}_s^2}\right)^{-N_L} f_v\left(\hat{r}_s\right) d\hat{r}_s, \tag{40}$$

where

$$g^{q}_{\mathrm{SB}}\left(s|\hat{r}_b\right) = \sum_{j=1}^{N_L} \binom{N_L}{j} (-1)^{j+1} \left(\frac{s\mathcal{P}_b C_L a_q^{vb}}{N_L}\right)^{j} \Bigg(\frac{\Gamma\left(1/2\right)\Gamma\left(j-1/2\right)}{2\Gamma\left(j\right)} \left(\mathrm{Z}_q\left(s\right)\right)^{\frac{1}{2}-j} - \frac{\hat{r}_b}{\left(\mathrm{Z}_q\left(s\right)\right)^{j}} {}_2F_1\left(\frac{1}{2}, j; \frac{1}{2}; -\frac{\hat{r}_b^2}{\mathrm{Z}_q\left(s\right)}\right)\Bigg). \tag{41}$$

and ${}_2F_1(.)$ is the Gaussian hypergeometric function.

Proof: With the aid of a special integral which is shown as follows

$$\int_0^{\hat{r}_b} \left(x^2+d\right)^{-j} dx = -\frac{\hat{r}_b}{d^j} {}_2F_1\left(\frac{1}{2}, j; \frac{1}{2}; -\frac{\hat{r}_b^2}{d}\right), \tag{42}$$

we obtain the closed-form expression for interference from LOS BSs. Note that the nearest PV is able to offer LOS interference. Therefore, we combine these two kinds of interference together to derive this corollary. ∎

2) Coverage Probability: Under the SB technique, the coverage probability is defined as

$$P_{\mathrm{SB}}\left(\Upsilon_{th}\right) = \mathbb{P}\left[\Upsilon_{\mathbf{x}_b} > \Upsilon_{th}\right]. \tag{43}$$

Theorem 2. *Under the SB technique, the coverage probability at the typical PV with a SINR threshold Υ_{th} is given by*

$$P_{\mathrm{SB}}\left(\Upsilon_{th}\right) \approx \sum_{k=1}^{N_L} (-1)^{k+1} \binom{N_L}{k} \int_{V_b}^{\infty} \exp\left(-kS_b^L\left(\hat{r}_b\right) n_0^2\right) \times \mathcal{L}_{\mathrm{SB}}\left(kS_b^L\left(\hat{r}_b\right)|\hat{r}_b\right) f_b^L\left(\hat{r}_b\right) d\hat{r}_b + \sum_{k'=1}^{N_N} (-1)^{k'+1} \binom{N_N}{k'} \times \int_{V_b}^{\infty} \exp\left(-k' S_b^N\left(\hat{r}_b\right) n_0^2\right) \mathcal{L}_{\mathrm{SB}}\left(k' S_b^N\left(\hat{r}_b\right)|\hat{r}_b\right) f_b^N\left(\hat{r}_b\right) d\hat{r}_b, \tag{44}$$

where $S_b^{\kappa}(\hat{r}_b) = \frac{\eta_\kappa \Upsilon_{th} \hat{r}_b^{\alpha_\kappa}}{\mathcal{P}_b G_m^v G_m^b C_\kappa}$.

Proof: The proof procedure is similar with **Theorem 1** *and hence we omit it here.* ∎

Corollary 9. *Under the special case, the* **Theorem 2** *can be simplified as follows:*

$$\tilde{P}_{\mathrm{SB}}\left(\Upsilon_{th}\right) \approx \sum_{k=1}^{N_L} (-1)^{k+1} \binom{N_L}{k} \int_{V_b}^{\infty} \exp\left(-kS_b^L\left(\hat{r}_b\right) n_0^2\right) \times \tilde{\mathcal{L}}_{\mathrm{SB}}\left(kS_b^L\left(\hat{r}_b\right)|\hat{r}_b\right) f_b^L\left(\hat{r}_b\right) d\hat{r}_b. \tag{45}$$

Proof: By replacing $\mathcal{L}_{\mathrm{SB}}(.)$ with $\tilde{\mathcal{L}}_{\mathrm{SB}}(.)$, we obtain this corollary. ∎

Remark 8. *Note that $f_b^L(.)$ in* (21) *has a positive correlation with λ_b, while $\tilde{\mathcal{L}}_{\mathrm{SB}}(.)$ is a monotonic decreasing function with λ_b. Under the SB technique, an optimal λ_b exists for maximizing the coverage probability $\tilde{P}_{\mathrm{SB}}\left(\Upsilon_{th}\right)$.*

Corollary 10. *For the heavy traffic, a closed-form expression for SNR coverage probability under the special case can be expressed as*

$$\ddot{P}_{\mathrm{SB}}\left(\Upsilon_{th}\right) \approx \sum_{k=1}^{N_L} (-1)^{k+1} \binom{N_L}{k} \frac{\lambda_b^L}{2} \sqrt{\frac{\pi}{C_7}} \times \exp\left(-C_7 V_b^2 + \frac{\left(\lambda_b^L\right)^2}{4C_7}\right)\left(1 - \mathrm{erf}\left(\frac{\lambda_b^L}{2\sqrt{C_7}}\right)\right), \tag{46}$$

where $C_7\left(\Upsilon_{th}\right) = \frac{k\eta_L \Upsilon_{th} n_0^2}{\mathcal{P}_v G_m^v G_m^b C_L}$.

Proof: Since NLOS transmission are ignored in this case, $f_b^L(\hat{r}_b)$ in **Lemma 3** *changes to be $\frac{\lambda_b^L \hat{r}_b}{\sqrt{\hat{r}_b^2 - V_b^2}} \exp\left(-\lambda_b^L \sqrt{\hat{r}_b^2 - V_b^2}\right)$ $(\hat{r}_b > V_b)$. With the similar process of* **Corollary 6**, *we obtain this corollary.* ∎

C. Strongest Transmitter Technique

In most cases, both roadside BSs and intra-lane PVs have same information. For example, all of them is capable of providing front road conditions to the typical PV. Since autonomous driving demands low outage probabilities to prevent 'losing control' for too long, it is reasonable to choose the transmitter (BS or PV) with the strongest received power to establish the communication link. Under the ST technique, the Laplace transform of interference for associating with the nearest PV is the same with the NP technique and for associating with the desired BS is the same with the SB technique. We directly derive expressions for coverage probabilities.

1) Coverage Probability: The coverage probability under the ST technique has three main parts as the typical PV is able to connect the nearest PV, the desired LOS BS, or the desired NLOS BS. Note that the desired transmitter is located at $\mathbf{x}_t$. The coverage probability in the ST technique is given by

$$P_{\mathrm{ST}}\left(\Upsilon_{th}\right)=\mathbb{P}\left[\Upsilon_{\mathbf{x}_t}>\Upsilon_{th}\right]. \tag{47}$$

Theorem 3. *Under the ST technique, the coverage probability at the typical PV with a SINR threshold Υ_{th} is given by*

$$\begin{aligned}P_{\mathrm{ST}}\left(\Upsilon_{th}\right)\approx&\sum_{k=1}^{N_L}\left(-1\right)^{k+1}\binom{N_L}{k}\Big(\int_{V_b}^{\infty}\exp\left(-kS_b^L\left(\hat{r}_t\right)n_0^2\right)\\&\times\mathcal{L}_{\mathrm{SB}}\left(kS_b^L\left(\hat{r}_t\right)|\hat{r}_t\right)f_t^L\left(\hat{r}_t\right)d\hat{r}_t\\&+\int_{d_P}^{\infty}\exp\left(-kS_v^L\left(\hat{r}_t\right)n_0^2\right)\mathcal{L}_{\mathrm{NP}}\left(kS_v^L a\left(\hat{r}_t\right)|\hat{r}_t\right)f_t^v\left(\hat{r}_t\right)d\hat{r}_t\Big)\\&+\sum_{k'=1}^{N_N}\left(-1\right)^{k'+1}\binom{N_N}{k'}\int_{V_b}^{\infty}\exp\left(-k'S_b^N\left(\hat{r}_t\right)n_0^2\right)\\&\times\mathcal{L}_{\mathrm{SB}}\left(k'S_b^N\left(\hat{r}_t\right)|\hat{r}_t\right)f_t^N\left(\hat{r}_t\right)d\hat{r}_t.\end{aligned} \tag{48}$$

Proof: The difference between the ST technique with other two techniques is the PDF of the communication distance. By replacing PDFs in **Theorem 1**, **Theorem 2** *with the PDFs from* **Lemma 4**, **Lemma 5**, *we obtain this theorem.* ∎

Corollary 11. *Under the special case, the* **Theorem 3** *can be simplified as follows*

$$\begin{aligned}\tilde{P}_{\mathrm{ST}}\left(\Upsilon_{th}\right)\approx&\sum_{k=1}^{N_L}\left(-1\right)^{k+1}\binom{N_L}{k}\Big(\int_{V_b}^{\infty}\exp\left(-kS_b^L\left(\hat{r}_t\right)n_0^2\right)\\&\times\tilde{\mathcal{L}}_{\mathrm{SB}}\left(kS_b^L\left(\hat{r}_t\right)|\hat{r}_t\right)f_t^L\left(\hat{r}_t\right)d\hat{r}_t\\&+\int_{d_P}^{\infty}\exp\left(-kS_v^L\left(\hat{r}_t\right)n_0^2\right)\tilde{\mathcal{L}}_{\mathrm{NP}}\left(kS_v^L a\left(\hat{r}_t\right)|\hat{r}_t\right)f_t^v\left(\hat{r}_t\right)d\hat{r}_t\Big).\end{aligned} \tag{49}$$

Proof: The Laplace transform of interference under the special case $\tilde{\mathcal{L}}_{\mathrm{NP}}(.)$ and $\tilde{\mathcal{L}}_{\mathrm{SB}}(.)$ are introduced to derive this corollary. Moreover, the cases that the typical PV connects to a NLOS BS are also ignored. ∎

Remark 9. *Note that when $x\to 0$, we have $\arcsin x\to x$, $\sin x\to x$. Based on this fact, when $N_\varrho\to\infty$, the expectation of antenna gains $\bar{G}_{v\varrho}\to\left(4+\frac{2}{3\pi}\right)^2\approx 4.21$. However, the maximum array gain $G_m^v G_m^\varrho$ is an increasing function with N_ϱ. By introducing these trends into* **Corollary 6**, **9**, **11**, *we conclude that large antenna arrays are able to enhance the coverage performance for all proposed techniques, namely NP, SB, and ST.*

Corollary 12. *For the heavy traffic, a tractable expression for SNR coverage probability under the special case can be expressed as*

$$\begin{aligned}\tilde{P}_{\mathrm{ST}}\left(\Upsilon_{th}\right)\approx&\sum_{k=1}^{N_L}\left(-1\right)^{k+1}\binom{N_L}{k}\Big(\int_{V_b}^{\infty}\exp\left(-kS_b^L\left(\hat{r}_t\right)n_0^2\right)\\&\times f_{ST}^b\left(\hat{r}_t\right)d\hat{r}_t+\int_{d_P}^{\infty}\exp\left(-kS_v^L\left(\hat{r}_t\right)n_0^2\right)\frac{\lambda_b^L\hat{r}_t}{\sqrt{\hat{r}_t^2-V_b^2}}\\&\times\exp\left(-\lambda_b^L\sqrt{\hat{r}_t^2-V_b^2}\right)\Big(1-f_{ST}^v\left(\frac{\hat{r}_t}{C_3^L}+D_1\right)\\&+f_{ST}^v\left(d_1^h\right)\Big)d\hat{r}_t\Big),\end{aligned} \tag{50}$$

where

$$\begin{aligned}f_{ST}^b\left(x\right)=&\frac{5d_1^h-D_1-x}{3d_1^h}\exp\Big(\frac{1-\ln(3d_1^h)-2\ln(2d_1^h)}{3}\\&-\lambda_b^L\sqrt{\left(C_3^L x\right)^2-V_b^2}-\frac{2\left(x+D_1\right)}{9d_1^h}\Big)\end{aligned} \tag{51}$$

$$\begin{aligned}f_{ST}^v\left(x\right)=&\frac{3}{4}\left(9+2x-10d_1^h\right)\\&\times\exp\big(\frac{1-\ln(3d_1^h)-2\ln(2d_1^h)}{3}-\frac{2x}{9d_1^h}\big).\end{aligned} \tag{52}$$

Proof: Note that BSs are able to provide more power and larger antenna scale than vehicles. Therefore, C_3^L in (23) *should obeys that $C_3^L>1$. Due to ignoring NLOS transmission, we have*

$$f_t^L\left(\hat{r}_t\right)\approx\left(1-\int_{d_P}^{\hat{r}_t/C_3^L}\dot{f}_{\rho_1}\left(x+D_1\right)dx\right)f_b^L\left(\hat{r}_t\right) \tag{53}$$

$$f_t^v(\hat{r}_t)\approx\exp\left(-\lambda_b^L\sqrt{\left(C_3^L\hat{r}_t\right)^2-V_b^2}\right)\dot{f}_{\rho_1}\left(\hat{r}_t+D_1\right). \tag{54}$$

By substituting (53) and (54) in **Corollary 11** *and deleting the interference part, we obtain this corollary.* ∎

V. Numerical Results

The general settings are presented in Tab. III. Regarding the thermal noise, it is decided by the absolute temperature and bandwidth. Assuming the bandwidth used in this system is $B_w=1$ GHz, the noise power n_0^2 is around -83 dBm. In the following part, we first validate the accuracy of proposed expressions and then provide further interesting insights.

A. Validating and Simulations

Since the exact PDF of the nearest distance r_s is intractable, an approximation formula has been provided in [39]. It regards an MHCP as a PPP that has the same density. However, the accuracy of this formula degrades when the density of the generating PPP λ_p increases. Therefore, we have derived a tighter approximation expression in **Proposition 1**. Moreover, two special cases have been provided as well. The comparison is shown in Fig. 3(a). For heavy traffic, namely $\lambda_p=\frac{1}{5}$, the analytical expression in **Corollary 2** and the tight lower

TABLE III
GENERAL SETTINGS OF THE PROPOSED NETWORKS [20]

Carrier frequency	$f_{\mathrm{mmW}} = 28$ GHz	**Intercept**	$C_L = C_N = -60$ dB
Path loss law for LOS	$\alpha_L = 2$, $N_L = 2$	**Path loss law for NLOS**	$\alpha_N = 4$, $N_N = 1$
Transmit Power	$\mathcal{P}_v = 1$ W, $\mathcal{P}_b = 10$ W	**Number of antennas**	$N_v = 2$, $N_b = 8$
Density	$\lambda_b = 1/50$, $\lambda_p = 1/5$ m^{-1}	**Length of vehicles**	$\tau = 5$ m
Width of lanes	$w_l = 5$ m	**Number of lanes**	$M = 3$
Safety distances	$d_M = 20$, $d_P = 10$ m	**Number of vehicles in one PV**	$n = 4$

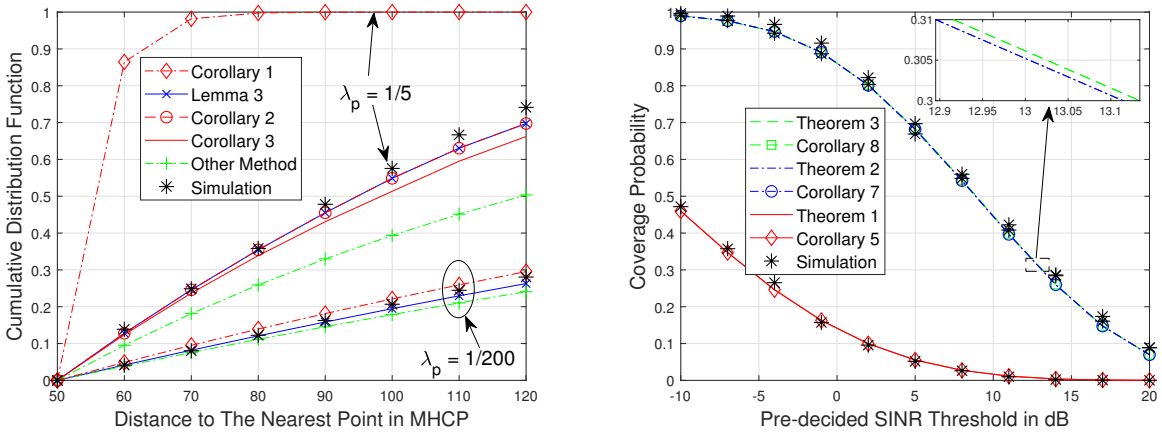

(a) (b)

Fig. 3. Validating and simulations with $P_i^H = 1$: (a) Appraising the accuracy of proposed approximations and comparing with the other technique [39], with a hard-core distance $d_h = 50$; (b) Coverage probability versus various SINR threshold Υ_{th}.

bound in **Corollary 3** have acceptable accuracy. Moreover, the CDF of the nearest distance in the heavy traffic case is independent of λ_p as mentioned in **Remark 4**. For light traffic, namely $\lambda_p = \frac{1}{200}$, **Corollary 1** performs better than the other technique in [39]. Although the gap between analytical results and simulations enlarges with the increase of the distance r_s as discussed in **Remark 3**, this flaw has a negligible impact on the coverage performance. The main reason is that when the communication distance between transceivers gradually elongates, the corresponding path loss augments rapidly. For the typical PV, the received SINR is mainly decided by the nearby transmitters.

Theorems and corollaries are appraised in Fig 3(b). In the figure, analytical results match simulations ideally, thereby validating the proposed approximation expressions. Furthermore, NLOS transmission can be ignored in the considered V2X networks since corollaries under the special case overlap the corresponding theorems.

B. Spatial Model for V2X Networks

In traditional V2X networks [25, 40], vehicles are modeled by multi-PPPs. Moreover, the blockage process is also derived by the PPP-based model [25]. However, this assumption is not accurate due to ignoring the length of vehicles, especially for platoons of autonomous vehicles. To evaluate the improvement of the proposed MHCP, we compare it with a PPP model with the same density, namely the compared PPP in the i-th lane has density $\lambda_p^c = \lambda_i$. As illustrated in Fig. 4(a), when the number of vehicles in one platoon obeys $n = 1$ (i.e., individual vehicles without forming platoons), the difference between two models is around 0.01 in the low Υ_{th} region. If networks being studied satisfy this condition, it is efficient to use PPP instead of MHCP. However, with the increase of n, the error becomes non-negligible. Regarding the high Υ_{th} region, the trend is the opposite. As a result, the PPP model for V2X networks is only practical when n is small in the low Υ_{th} region or n is large in the high Υ_{th} region. For the rest scenarios, MHCP is a better choice. In addition, small n benefits the coverage performance of the typical PV.

As shown in Fig. 4(b), for the NP technique, the coverage probability has a negative correlation with the density of BSs λ_b. For the SB technique, there exists an optimal λ_b as discussed in **Remark 8**. In auto-driving scenarios, the coverage probability of unmanned vehicles should be high otherwise it may be out of control. As a result, if the SINR threshold obeys $\Upsilon = 0$ dB, when λ_b is small, the controlled PV should be connected to the nearest PV, while when λ_b is large, the SB technique is a better choice. Since the ST technique is not sensitive to the density of BSs, it is able to achieve the best performance but at a cost of extra hand-offs. Moreover, a large number of blocking lanes $(M-1)$ benefits the NP technique but impairs the other two techniques.

C. MmWave Properties

For mmWave communications, the scale of antennas is an important factor. Although enlarging the number of antenna elements enhances the interference via the main beam, the probability of this condition, namely the main beam width θ_m^o, is reduced. Fig. 5(a) demonstrates that coverage probabilities have a positive correlation with both the scale of antennas at

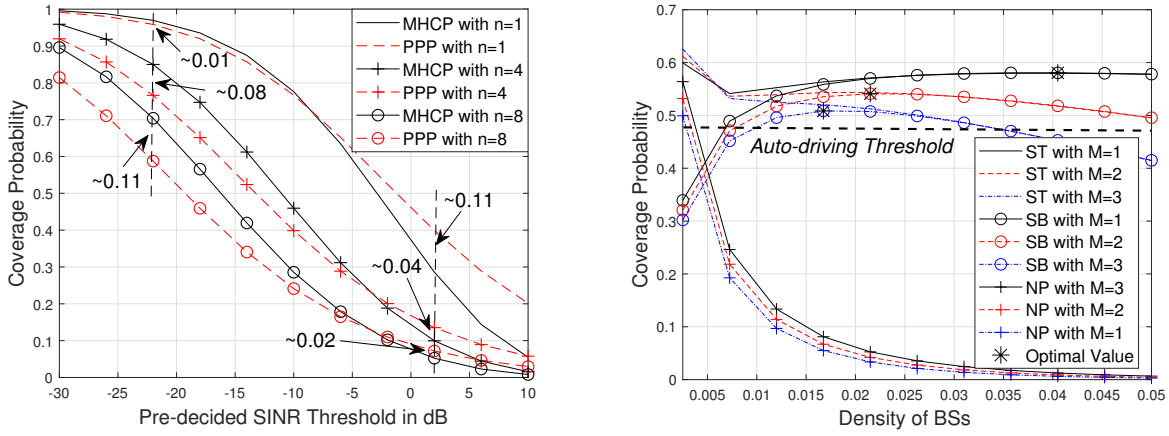

(a) (b)

Fig. 4. Spatial model analysis with $P_i^H = 1$: (a) Coverage probability versus various SINR threshold Υ_{th}, with the comparison with a same density PPP under the NP technique; (b) Coverage probability versus various densities of BSs, with $N_b = 2$ and the SINR threshold $\Upsilon_{th} = 0$ dB.

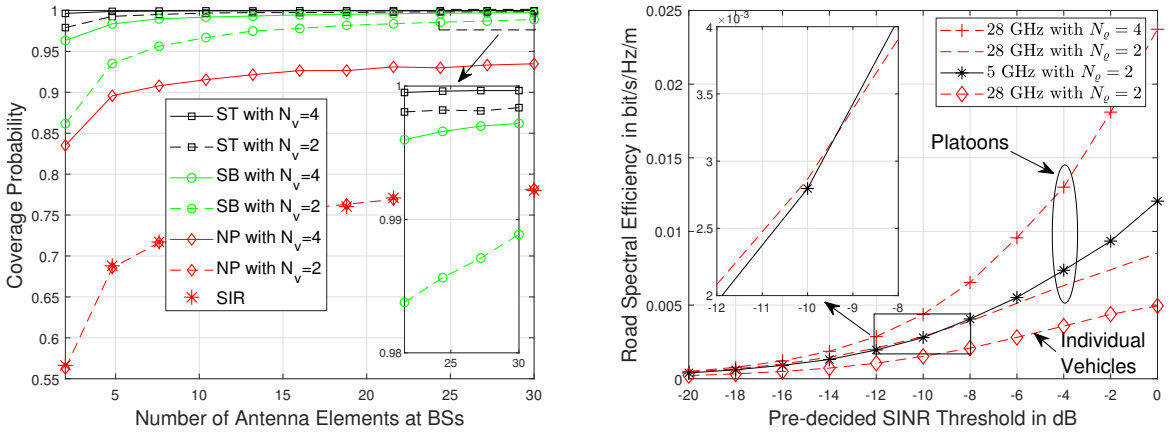

(a) (b)

Fig. 5. MmWave properties analysis with $P_i^H = 1$: (a) Coverage probability versus various number of antenna settings, with $\Upsilon_{th} = -10$ dB, the density of BSs $\lambda_b = 1/100$, the BS transmit power $P_b = 5$ W, and the number of vehicles in one PV $n = 5$; (b) Coverage probability versus various SINR threshold Υ_{th}, with $P_b = 5$ W, $\lambda_b = 1/100$, $\lambda_p = 1/50$, $n = 1$ (individual vehicles), $n = 3$ (platoons), $N_L = N_N = 1$ (sub-6 GHz), $\lambda_L = \lambda_N = 3$ (sub-6 GHz), and $N_L = 3$, $N_N = 2$ (mmWave).

BSs N_b and vehicles N_v under all techniques as discussed in **Remark 9**. The increasing trend becomes stable when $N_b > 10$. Regarding the considered thermal noise, it is essentially weaker than the interference in our system. To compare the performance before and after applying platoons, we introduce a new metric named road spectral efficiency (RSE), which evaluates the spectral efficiency in a unit length. Since three techniques have the same characteristic in terms of RSE, we only discuss RSE under the NP technique here, which equals to $\lambda_1 \log_2(1+\Upsilon_{th}) P_{\mathrm{NP}}(\Upsilon_{th})$ with a unit bit/s/Hz/m. Fig. 5(b) shows that platoons help to increase the RSE due to obtaining a higher density as mentioned in **Remark 2**. Fig. 5(b) also illustrates that although the improvement of the coverage performance is limited when upgrading sub-6 GHz to mmWave, with the increase of antenna scale, the advantage of mmWave communications becomes outstanding.

VI. Conclusion

This paper has created a tractable spatial model for platoon-based mmWave V2X networks with the aid of MHCPs. Based on this model, we have derived several closed-form expressions for the PDFs of various communication distances. Additionally, we have analytically evaluated coverage probabilities for three practical user association techniques. Numerical results have shown that the ST technique is an effective user association scheme in the physical layer for guaranteeing the auto-driving requirement. The possible further research directions are advanced beam tracking techniques and the analysis for other kinds of delay, e.g, processing delay, queuing delay, transmission delay, etc.

Appendix A: Proof of Lemma 1

As illustrated in Fig. 6(a), we first consider the case that $M = 2$. Assuming the receiving antenna in the 1-st lane is located at $\mathbf{x}_r$ and the transmitting antenna in the 3-rd 'lane'

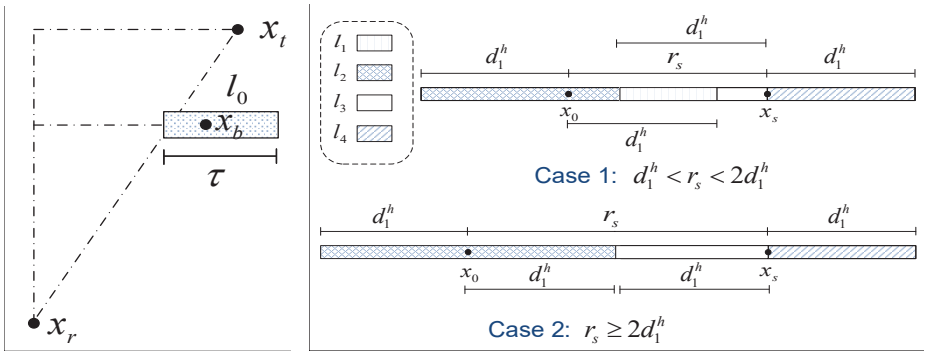

(a) (b)

Fig. 6. Figures for proofs: (a) Blockage process with one lane between the transmitter and receiver; (b) Classification of line segments under two cases.

is at $\mathbf{x}_t$, the LOS transmission between these two antennas is obstructed only if there is a blocking vehicle located in the region l_0 of the 2-nd lane. The blocking vehicle at $\mathbf{x}_b$ has a height of $H_{\mathbf{x}_b}$ and the length of l_0 equals to the length of one vehicle, namely τ. Under this case, the probability of no being blocked can be expressed as

$$\begin{aligned} P_L(2) =& 1-\mathbb{P}[\Phi_2 \cap l_0 = x_b, H_{\mathbf{x}_b} \geq H_2] \\ =& 1-P_2^H \mathbb{P}[\Phi_p \cap l_0 \neq \emptyset, \Phi_2 \cap \Phi_p = x_b] \\ \overset{(a)}{=}& 1-P_2^H \sum_{k=1}^{\infty} \binom{k}{1} \frac{(\lambda_p \tau)^k}{k!} \exp(-\lambda_p \tau) P_{\mathrm{re}}(d_2^h) \\ \overset{(b)}{=}& 1-P_2^H \lambda_2 \tau, \end{aligned} \tag{A.1}$$

where (a) follows the fact $\tau < d_2^h$, which means only one generating points from Φ_p can be retained in the region l_0 due to the definition of MHCP. Therefore, the probability for the point $\mathbf{x}_b$ being retained is $P_{\mathrm{re}}(d_2^h)$. The process (b) follows the power series of exponential function, namely $\exp(x) = \sum_{k=0}^{\infty} \frac{x^k}{k!}$.

For multi-lane cases $(M > 2)$, since the point distribution in each lane is independent and the probability $P_L(M)$ has no relationship with the horizontal communication distance (as shown in (A.1)), we obtain that

$$P_L(M) = \prod_{i=1}^{M-1} (1 - P_i^H \lambda_i \tau). \tag{A.2}$$

For the single-lane case $(M = 1)$, there is no blocking MVs and hence the probability of LOS transmission equals one, namely $P_L(1) = 1$.

Combining aforementioned cases, we have **Lemma 1**. Then, the proof is complete.

Appendix B: Proof of Lemma 2

In the MHCP Φ_1, we assume that for one point at $\mathbf{x} = (X_{\mathbf{x}}, Y_{\mathbf{x}})$ $(\mathbf{x} \in \Phi_1)$, its *safety region* $\mathbb{L}_{\mathbf{x}}$ is from $(X_{\mathbf{x}} - d_1^h, Y_{\mathbf{x}})$ to $(X_{\mathbf{x}} + d_1^h, Y_{\mathbf{x}})$. In order to demonstrate intuitively, four kinds of line segments are introduced as shown in Fig. 6(b). They are defined as follows:

- l_1: the intersection of two safety regions $\mathbb{L}_{\mathbf{x}_0}$ and $\mathbb{L}_{\mathbf{x}_s}$, namely $l_1 = \mathbb{L}_{\mathbf{x}_0} \cap \mathbb{L}_{\mathbf{x}_s}$.
- l_2: the complement of $\mathbb{L}_{\mathbf{x}_0}$, namely $l_2 = \mathbb{L}_{\mathbf{x}_0} \backslash l_1$.
- l_3: the void range from $(X_{\mathbf{x}_0} + d_1^h, Y_{\mathbf{x}_0})$ to $\mathbf{x}_s$. No point is located in this range as the point at $\mathbf{x}_s$ is the nearest one to $\mathbf{x}_0$.
- l_4: the complement of $\mathbb{L}_{\mathbf{x}_s}$, namely $l_4 = \mathbb{L}_{\mathbf{x}_s} \backslash l_1, l_3$.

Therefore, the corresponding thinning probability $\rho_1(r_s)$ is defined as [41]:

$$\begin{aligned} \rho_1(r_s) &= \mathbb{P}\left[\mathbf{x}_s \in \Phi_1 | \Phi_1 \cap l_3 = \emptyset, \mathbf{x}_0 \in \Phi_1\right] \\ &\overset{(a)}{\approx} \frac{\mathbb{P}\left[\mathbf{x}_s \in \Phi_1 \cap \mathbf{x}_0 \in \Phi_1 \,|\Phi_p \cap l_3 = \emptyset\right]}{\mathbb{P}\left[\mathbf{x}_0 \in \Phi_1 \,|\Phi_p \cap l_3 = \emptyset\right]} = \frac{\Theta_1(r_s)}{\Theta_2}, \end{aligned} \tag{B.1}$$

where (a) follows the fact that in a limited region l_3, MHCP Φ_1 can be tightly approximated by its generating PPP Φ_p. Since $(x_0 \in \Phi_1)$ is independent of the condition $(\Phi_p \cap l_3 = \emptyset)$, we have

$$\Theta_2 = P_{\mathrm{re}} = \frac{1 - \exp(-2\lambda_p d_1^h)}{2\lambda_p d_1^h}. \tag{B.2}$$

Note that the nature of MHCP is that $r_s > d_1^h$. Regarding $\Theta_1(r_s)$, it is obvious that when $r_s \leq d_1^h$, $\Theta_1(r_s) = 0$. For $r_s > d_1^h$, it can be analyzed under two cases (see Fig. 6(b)): **Case 1**, where $d_1^h < r_s < 2d_1^h$; and **Case 2**, where $r_s \geq 2d_1^h$.

For **Case 1**, if the marks for $\mathbf{x}_0$ and $\mathbf{x}_s$ are $m_{\mathbf{x}_0}$ and $m_{\mathbf{x}_s}$, respectively, $\Theta_1(r_s)$ is given at the top of next page, where (b) holds the fact that for a point $\mathbf{x}_s \in \Phi_p$ with a mark $m_{\mathbf{x}_s}$, the probability for retaining this point in a region $l \subseteq \mathbb{L}_{\mathbf{x}_s}$ is $\exp(-m_{\mathbf{x}_s} \lambda_p l)$. We introduce a special integral as follows:

$$\begin{aligned} f_n(a,b) &= \int_0^1 \exp(-\lambda_p a t_0) \int_0^{t_0} \exp(-\lambda_p b t) dt dt_0 \\ &= \frac{1 - \exp(-\lambda_p a)}{\lambda_p^2 ab} - \frac{1 - \exp(-\lambda_p (a+b))}{\lambda_p^2 (a+b) b}. \end{aligned} \tag{B.4}$$

By substituting (B.4) into (B.3), we obtain that

$$\Theta_1(r_s) = f_n(2d_1^h, d_1^h) + f_n((3d_1^h - r_s), r_s). \tag{B.5}$$

For **Case 2**, we have $l_1 \cup l_2 = 2d_1^h$, $l_4 = d_1^h$, $l_2 = 2d_1^h$, and $l_2 \cup l_4 = d_1^h$. With the similar proof procedure in (B.3), Θ_1 can be expressed as

$$\Theta_1(r_s) = f_n(2d_1^h, d_1^h) + f_n(d_1^h, 2d_1^h). \tag{B.6}$$

By substituting (B.2), (B.5), and (B.6) into (B.1), we have **Lemma 2**. Then, the proof is completed.

$$\begin{aligned}\Theta_1(r_s) =&\mathbb{P}\left[(l_1\cup l_2)\cap\Phi_1=\mathbf{x}_0, l_4\cap\Phi_1=\mathbf{x}_s\,|\Phi_p\cap l_3=\emptyset, m_{\mathbf{x}_0}>m_{\mathbf{x}_s}\right]\\ &+\mathbb{P}\left[l_2\cap\Phi_1=\mathbf{x}_0, (l_1\cup l_4)\cap\Phi_1=\mathbf{x}_s\,|\Phi_p\cap l_3=\emptyset, m_{\mathbf{x}_0}\le m_{\mathbf{x}_s}\right]\\ \overset{(b)}{=}&\int_0^1\exp\left(-2m_{\mathbf{x}_0}\lambda_p d_1^h\right)\int_0^{m_{\mathbf{x}_0}}\exp\left(-m_{\mathbf{x}_s}\lambda_p d_1^h\right)dm_{\mathbf{x}_s}dm_{\mathbf{x}_0}\\ &+\int_0^1\exp\left(-m_{\mathbf{x}_s}\lambda_p\left(3d_1^h-r\right)\right)\int_0^{m_{\mathbf{x}_s}}\exp\left(-m_{\mathbf{x}_0}\lambda_p r\right)dm_{\mathbf{x}_0}dm_{\mathbf{x}_s},\end{aligned}\tag{B.3}$$

Appendix C: Proof of Lemma 3

In the $(M+1)$-th 'lane', the probability of the typical PV not being blocked is $P_L(M)$. Therefore, the density for LOS and NLOS BSs are $\lambda_b^L=\lambda_b P_L(M)$ and $\lambda_b^N=\lambda_b P_N(M)$, respectively. Let the nearest LOS BS is located at $\mathbf{x}_b^L\in\Phi_{M+1}$ and the counterpart for NLOS BS is $\mathbf{x}_b^N\in\Phi_{M+1}$. Then, the corresponding communication distance for LOS and NLOS BS are $r_b^L=\|\mathbf{x}_b^L\|$ and $r_b^N=\|\mathbf{x}_b^N\|$, respectively. Both r_b^L and r_b^N should be larger than the vertical coordinate V_b. The typical PV should be associated with LOS transmitter if $(C_L {r_b^L}^{-\alpha_L}\ge C_N {r_b^N}^{-\alpha_N})$. Hence, the PDF for the typical vehicle associating with a LOS MV is given by

$$f_b^L(\hat{r}_b)=\mathbb{P}[C_L\hat{r}_b^{-\alpha_L}\ge C_N\left(r_b^N\right)^{-\alpha_N},\hat{r}_b=r_b^L].\tag{C.1}$$

Since $r_b^N\ge V_b$, the minimum distance for LOS transmission is $\Pi_{\rm th}$. When $V_b<r_b^L<\Pi_{\rm th}$, the $f_b^L(\hat{r}_b)$ equals to the PDF of nearest LOS distance, which can be expressed as [20]

$$f_b^L(\hat{r}_b)=\frac{\lambda_b^L\hat{r}_b}{\sqrt{\hat{r}_b^2-V_b^2}}\exp\left(-\lambda_b^L\sqrt{\hat{r}_b^2-V_b^2}\right).\tag{C.2}$$

When $r_b^L\ge\Pi_{\rm th}$, the $f_b^L(\hat{r}_b)$ can be calculated with the aid of (C.1), which is given by

$$\begin{aligned}f_b^L(\hat{r}_b)=&\mathbb{P}[C_L\hat{r}_b^{-\alpha_L}\ge C_N\left(r_b^N\right)^{-\alpha_N},\hat{r}_b=r_b^L]\\ =&\mathbb{P}[(r_b^N)\ge\Pi_L\left(\hat{r}_b\right),\hat{r}_b=r_b^L]\\ =&\frac{\lambda_b^L\hat{r}_b}{\sqrt{\hat{r}_b^2-V_b^2}}\exp\left(-\lambda_b^L\sqrt{\hat{r}_b^2-V_b^2}\right)\\ &\times\exp\left(-\lambda_b^N\sqrt{\Pi_L^2\left(\hat{r}_b\right)-V_b^2}\right).\end{aligned}\tag{C.3}$$

With the similar proof procedure, we obtain the PDF for the typical PV associating with a NLOS BS. Then the proof is completed.

Appendix D: Proof of Proposition 2

For the NP technique, there exist two kinds of interference, which are intra-lane interference $I_{\rm intra}^{\rm NP}$ and interference from BSs $I_{\rm BS}^{\rm NP}$. When the interferer is located at $\mathbf{x}$, the corresponding Laplace transform of interference can be defined as

$$\mathcal{L}_{\rm NP}\left(s\,|\hat{r}_s\right)=\mathbb{E}\left[\exp\left(-s\left(I_{\rm intra}^{\rm NP}+I_{\rm BS}^{\rm NP}\right)\right)|\hat{r}_s=\|\mathbf{x}_s\|-D_1\right],\tag{D.1}$$

where

$$I_{\rm intra}^{\rm NP}=\sum_{\mathbf{x}\in\Phi_1\setminus\mathbf{x}_0,\mathbf{x}_s}\mathcal{P}_v\mathrm{L}\left(0,\|\mathbf{x}\|-D_1\right)G_{\mathbf{x}}\left|h_{\mathbf{x}}\right|^2,\tag{D.2}$$

$$I_{\rm BS}^{\rm NP}=\sum_{\mathbf{x}\in\Phi_{M+1}}\mathcal{P}_b\mathrm{L}\left(M,\|\mathbf{x}\|\right)G_{\mathbf{x}}\left|h_{\mathbf{x}}\right|^2.\tag{D.3}$$

Regarding the $I_{\rm intra}^{\rm NP}$, since the desired device is included in the same lane, the Laplace transform of $I_{\rm intra}^{\rm NP}$ should conditional on $\hat{r}_s$. Therefore, we have (D.4) at the top of next page, where (a) utilizes Jensen's inequality. (b) applies the Campbell's theorem into the MHCP $\Phi_1\setminus\mathbf{x}_0$ [30] and the origin point changes to $\mathbf{x}_s$. (c) computes the expectation of antenna gain $G_{\mathbf{x}}$ and a gamma variable $|h_{\mathbf{x}}|^2$.

Based on the probability generating functional of a PP-P [18], it is effortless to derive the Laplace transform of $I_{\rm BS}^{\rm NP}$ and it is as follows

$$\begin{aligned}L_{\rm BS}^{\rm NP}(s)=&\mathbb{E}[\exp(-s\sum_{\mathbf{x}\in\Phi_{M+1}}\mathcal{P}_b\mathrm{L}\left(M,\|\mathbf{x}\|\right)G_{\mathbf{x}}|h_{\mathbf{x}}|^2)]\\ =&\prod_{q=1}^{4}\mathcal{L}_{V_L}^q(s)\,\mathcal{L}_{V_N}^q(s).\end{aligned}\tag{D.5}$$

Then, the proof is completed.

References

[1] W. Yi, Y. Liu, and A. Nallanathan, "Coverage analysis for mmWave-enabled V2X networks via stochastic geometry," in *IEEE Proc. of Global Commun. Conf. (GLOBECOM)*, Dec. 2019.

[2] J. Choi, V. Va, N. Gonzalez-Prelcic, R. Daniels, C. R. Bhat, and R. W. Heath, "Millimeter-wave vehicular communication to support massive automotive sensing," *IEEE Commun. Mag.*, vol. 54, no. 12, pp. 160–167, Dec. 2016.

[3] R. Hall and C. Chin, "Vehicle sorting for platoon formation: Impacts on highway entry and throughput," *Transportation Research Part C: Emerging Technologies*, vol. 13, no. 5-6, pp. 405–420, 2005.

[4] H. Meinel and A. Plattner, "Millimetre-wave propagation along railway lines," *IEE Proc. F - Commun., Radar and Signal Process.*, vol. 130, no. 7, pp. 688–694, December 1983.

[5] S. Tsugawa, "Issues and recent trends in vehicle safety communication systems," *IATSS research*, vol. 29, no. 1, pp. 7–15, 2005.

[6] V. Va, T. Shimizu, G. Bansal, R. W. Heath Jr *et al.*, "Millimeter wave vehicular communications: A survey," *Foundations and Trends® in Networking*, vol. 10, no. 1, pp. 1–113, 2016.

[7] V. *et al*, "5G automotive vision," 5G Infrastructure Public Private Partnership (5G PPP), White paper, Oct. 2015.

[8] D. Jia, K. Lu, J. Wang, X. Zhang, and X. Shen, "A survey on platoon-based vehicular cyber-physical systems," *IEEE Commun. Surveys Tutorials*, vol. 18, no. 1, pp. 263–284, Firstquarter 2016.

[9] K. Liang, J. Martensson, and K. H. Johansson, "Heavy-duty vehicle platoon formation for fuel efficiency," *IEEE Trans. Intell. Transp. Syst.*, vol. 17, no. 4, pp. 1051–1061, Apr. 2016.

[10] C. Nowakowski, J. O'Connell, S. E. Shladover, and D. Cody, "Cooperative adaptive cruise control: Driver acceptance of following gap settings less than one second," in *Proceedings of the Human Factors and Ergonomics Society Annual Meeting*, vol. 54, no. 24. SAGE Publications Sage CA: Los Angeles, CA, 2010, pp. 2033–2037.

[11] T. S. Rappaport, J. N. Murdock, and F. Gutierrez, "State of the art in 60-GHz integrated circuits and systems for wireless communications," *Proc. of the IEEE*, vol. 99, no. 8, pp. 1390–1436, Aug 2011.

[12] Y. Yu, P. G. Baltus, and A. H. Van Roermund, *Integrated 60GHz RF beamforming in CMOS*. Springer Science & Business Media, 2011.

$$\mathcal{L}_{\text{intra}}^{\text{NP}}\left(s\left|\hat{r}_s\right.\right)=\mathbb{E}\left[\exp\left(-s\sum_{\mathbf{x}\in\Phi_1\setminus\mathbf{x}_0,\mathbf{x}_s}\mathcal{P}_v\mathrm{L}\left(0,\|\mathbf{x}\|-D_1\right)G_{\mathbf{x}}\left|h_{\mathbf{x}}\right|^2\right)\left|\hat{r}_1\right.\right]$$
$$\overset{(a)}{\approx}\exp\left(-s\mathbb{E}\left[\sum_{\mathbf{x}\in\Phi_1\setminus\mathbf{x}_0,\mathbf{x}_s}\mathcal{P}_v\mathrm{L}\left(0,u+\hat{r}_s\right)G_{\mathbf{x}}\left|h_{\mathbf{x}}\right|^2\left|u=\|\mathbf{x}-\mathbf{x}_s\|\right.\right]\right)$$
$$\overset{(b)}{=}\exp\left(-\frac{s\mathcal{P}_vC_N}{\lambda_1}\int_{d_1^h}^{\infty}\lambda_1^{(2)}\left(u\right)\mathbb{E}\left[\left(u+\hat{r}_s\right)^{-\alpha_N}G_x|h_{\mathbf{x}}|^2\right]du\right)$$
$$\overset{(c)}{=}\exp\left(-\frac{s\mathcal{P}_vC_N\bar{G}_{vv}}{\lambda_1}\int_{d_1^h}^{\infty}\lambda_1^{(2)}\left(u\right)\left(u+\hat{r}_s\right)^{-\alpha_N}du\right), \tag{D.4}$$

[13] D. Fritsche, G. Tretter, C. Carta, and F. Ellinger, "Millimeter-wave low-noise amplifier design in 28-nm low-power digital CMOS," *IEEE Trans. on Microw. Theory and Techn.*, vol. 63, no. 6, pp. 1910–1922, Jun. 2015.

[14] E. Zochmann, M. Hofer, M. Lerch, S. Pratschner, L. Bernado, J. Blumenstein, S. Caban, S. Sangodoyin, H. Groll, T. Zemen, A. Prokes, M. Rupp, A. F. Molisch, and C. F. Mecklenbrauker, "Position-specific statistics of 60 GHz vehicular channels during overtaking," *IEEE Access*, vol. 7, pp. 14 216–14 232, 2019.

[15] V. Petrov, G. Fodor, J. Kokkoniemi, D. Moltchanov, J. Lehtomaki, S. Andreev, Y. Koucheryavy, M. Juntti, and M. Valkama, "On unified vehicular communications and radar sensing in millimeter-wave and low terahertz bands," *IEEE Wireless Commun.*, vol. 26, no. 3, pp. 146–153, Jun. 2019.

[16] Y. Wang, A. Klautau, M. Ribero, M. Narasimha, and R. W. Heath, "Mmwave vehicular beam training with situational awareness by machine learning," in *IEEE Globecom Workshops (GC Wkshps)*, Dec 2018, pp. 1–6.

[17] A. Ghosh, T. A. Thomas, M. C. Cudak, R. Ratasuk, P. Moorut, F. W. Vook, T. S. Rappaport, G. R. MacCartney, S. Sun, and S. Nie, "Millimeter-wave enhanced local area systems: A high-data-rate approach for future wireless networks," *IEEE J. Sel. Areas Commun.*, vol. 32, no. 6, pp. 1152–1163, Jun. 2014.

[18] W. Yi, Y. Liu, and A. Nallanathan, "Cache-enabled hetnets with millimeter wave small cells," *IEEE Trans. Commun.*, vol. 66, no. 11, pp. 5497–5511, Nov. 2018.

[19] M. Haenggi, *Stochastic geometry for wireless networks*. Cambridge University Press, 2012.

[20] T. Bai and R. W. Heath, "Coverage and rate analysis for millimeter-wave cellular networks," *IEEE Trans. Wireless Commun.*, vol. 14, no. 2, pp. 1100–1114, Feb. 2015.

[21] H. Elshaer, M. N. Kulkarni, F. Boccardi, J. G. Andrews, and M. Dohler, "Downlink and uplink cell association with traditional macrocells and millimeter wave small cells," *IEEE Trans. Wireless Commun.*, vol. 15, no. 9, pp. 6244–6258, Sep. 2016.

[22] W. Yi, Y. Liu, and A. Nallanathan, "Modeling and analysis of D2D millimeter-wave networks with Poisson cluster processes," *IEEE Trans. Commun.*, vol. 65, no. 12, pp. 5574–5588, Dec. 2017.

[23] Y. Wang, K. Venugopal, A. F. Molisch, and R. W. Heath, "Mmwave vehicle-to-infrastructure communication: Analysis of urban microcellular networks," *IEEE Trans. Veh. Technol.*, vol. 67, no. 8, pp. 7086–7100, Aug. 2018.

[24] V. V. Chetlur and H. S. Dhillon, "Coverage analysis of a vehicular network modeled as cox process driven by poisson line process," *IEEE Trans. Wireless Commun.*, vol. 17, no. 7, pp. 4401–4416, Jul. 2018.

[25] A. Tassi, M. Egan, R. J. Piechocki, and A. Nix, "Modeling and design of millimeter-wave networks for highway vehicular communication," *IEEE Trans. Veh. Technol.*, vol. 66, no. 12, pp. 10 676–10 691, Dec. 2017.

[26] Y. J. Cho, K. Huang, and C. Chae, "V2X downlink coverage analysis with a realistic urban vehicular model," in *IEEE Globecom Workshops (GC Wkshps)*, Dec. 2018, pp. 1–6.

[27] F. J. Martłn-Vega, B. Soret, M. C. Aguayo-Torres, I. Z. Kovcs, and G. Gmez, "Geolocation-based access for vehicular communications: Analysis and optimization via stochastic geometry," *IEEE Trans. Veh. Technol.*, vol. 67, no. 4, pp. 3069–3084, Apr. 2018.

[28] Y. Wang, K. Venugopal, A. F. Molisch, and R. W. Heath, "Blockage and coverage analysis with mmWave cross street BSs near urban intersections," in *IEEE Proc. of International Commun. Conf. (ICC)*, May 2017, pp. 1–6.

[29] B. Matérn, *Spatial variation*. Springer Science & Business Media, 2013, vol. 36.

[30] A. M. Ibrahim, T. ElBatt, and A. El-Keyi, "Coverage probability analysis for wireless networks using repulsive point processes," in *2013 IEEE 24th Annual International Symposium on Personal, Indoor, and Mobile Radio Communications (PIMRC)*, Sep. 2013, pp. 1002–1007.

[31] J. Illian, A. Penttinen, H. Stoyan, and D. Stoyan, *Statistical analysis and modelling of spatial point patterns*. John Wiley & Sons, 2008, vol. 70.

[32] W. Yi, Y. Liu, A. Nallanathan, and M. Elkashlan, "Clustered millimeter wave networks with non-orthogonal multiple access," *IEEE Trans. Commun.*, vol. 67, no. 6, pp. 4350–4364, Jun. 2019.

[33] X. Yu, J. Zhang, M. Haenggi, and K. B. Letaief, "Coverage analysis for millimeter wave networks: The impact of directional antenna arrays," *IEEE J. Sel. Areas Commun.*, vol. 35, no. 7, pp. 1498–1512, Jul. 2017.

[34] S. Wei, Y. Zou, X. Zhang, T. Zhang, and X. Li, "An integrated longitudinal and lateral vehicle following control system with radar and vehicle-to-vehicle communication," *IEEE Trans. Veh. Technol.*, vol. 68, no. 2, pp. 1116–1127, Feb. 2019.

[35] S. Ucar, S. C. Ergen, and O. Ozkasap, "IEEE 802.11p and visible light hybrid communication based secure autonomous platoon," *IEEE Trans. Veh. Technol.*, vol. 67, no. 9, pp. 8667–8681, Sep. 2018.

[36] S. Rangan, T. S. Rappaport, and E. Erkip, "Millimeter-wave cellular wireless networks: Potentials and challenges," *Proc. of the IEEE*, vol. 102, no. 3, pp. 366–385, Mar. 2014.

[37] Z. Pi and F. Khan, "An introduction to millimeter-wave mobile broadband systems," *IEEE Commun. Mag.*, vol. 49, no. 6, pp. 101–107, Jun. 2011.

[38] A. Jeffrey and D. Zwillinger, *Table of integrals, series, and products*. Academic press, 2007.

[39] Y. Zhu, G. Zheng, and M. Fitch, "Secrecy rate analysis of UAV-enabled mmwave networks using Matérn hardcore point processes," *IEEE J. Sel. Areas Commun.*, vol. 36, no. 7, pp. 1397–1409, July 2018.

[40] M. J. Farooq, H. ElSawy, and M. Alouini, "A stochastic geometry model for multi-hop highway vehicular communication," *IEEE Trans. Wireless Commun.*, vol. 15, no. 3, pp. 2276–2291, Mar. 2016.

[41] A. Al-Hourani, R. J. Evans, and S. Kandeepan, "Nearest neighbor distance distribution in hard-core point processes," *IEEE Commun. Lett.*, vol. 20, no. 9, pp. 1872–1875, Sep. 2016.